John Barnard
Steven Lund
USPAS
June 2008

An application of intense beams

1. Heavy-ion fusion
   A. Requirements
   B. Targets for ICF
   C. Accelerator
   D. Drift compression
   E. Final focus
   F. Experiments

Inertial Fusion Energy (IFE) power plants of the future will consist of four parts

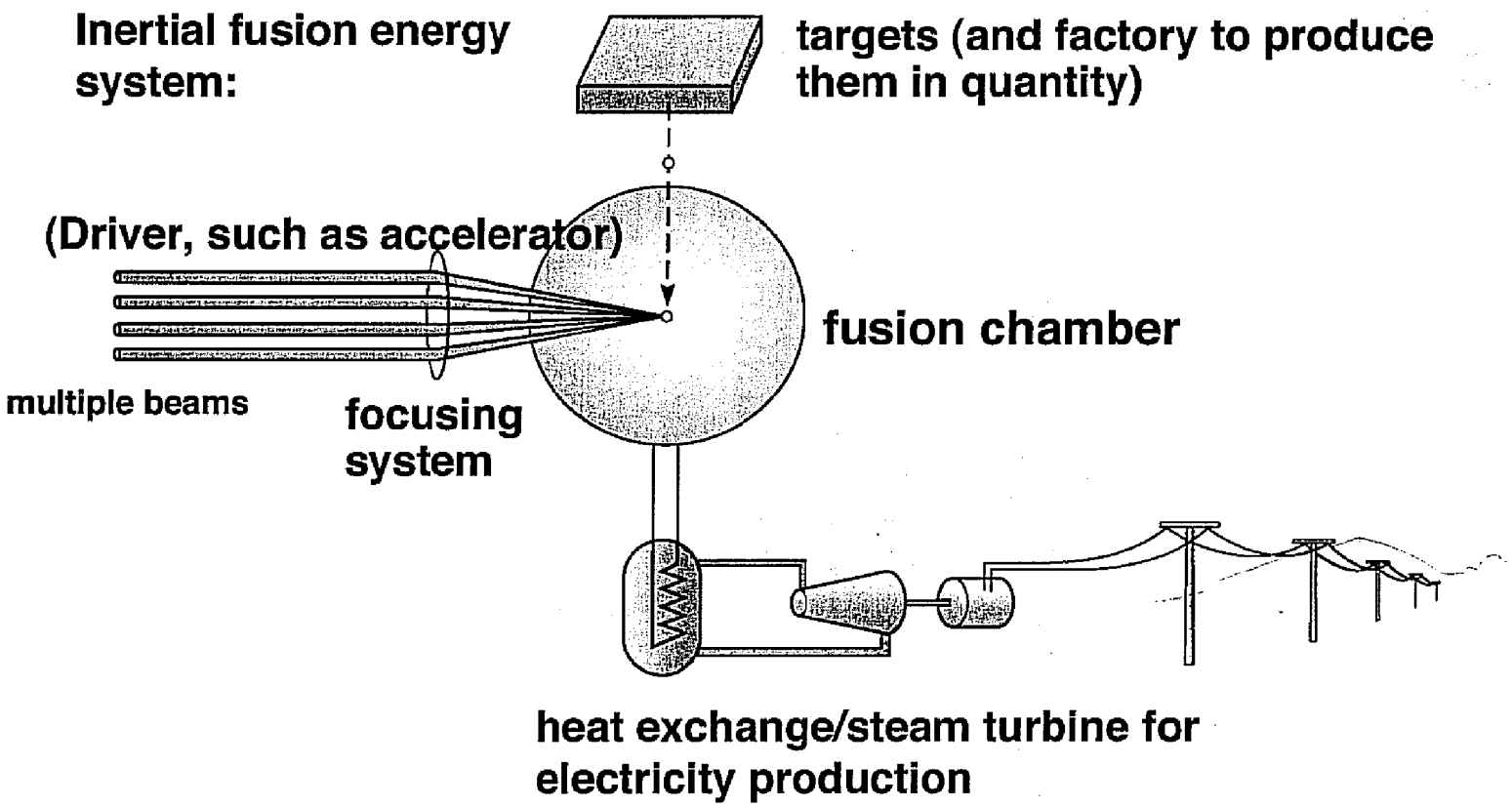

Heavy Ion Fusion provides an attractive approach to long term energy production

Fusion offers an inexaustible, long term solution to the problem of future energy supplies free from long-lived radioactive by-products and greenhouse CO_2.

Inertial Confinement Fusion (ICF) uses laser or particle beams to implode a target, raising the temperature and density of the fuel, creating the conditions necessary for the following reaction:

$$D + T \rightarrow n\ (14.06\ MeV) + He^4\ (3.52\ MeV)\ .$$

Heavy ion accelerators are a strong candidate for inertial fusion *energy production* (IFE) because of:

- High efficiency
- High repetition rate
- Survivability of final lens
- Favorable target illumination geometry

National Ignition Facility has 192 beams of 40-cm aperture arranged in four beam clusters

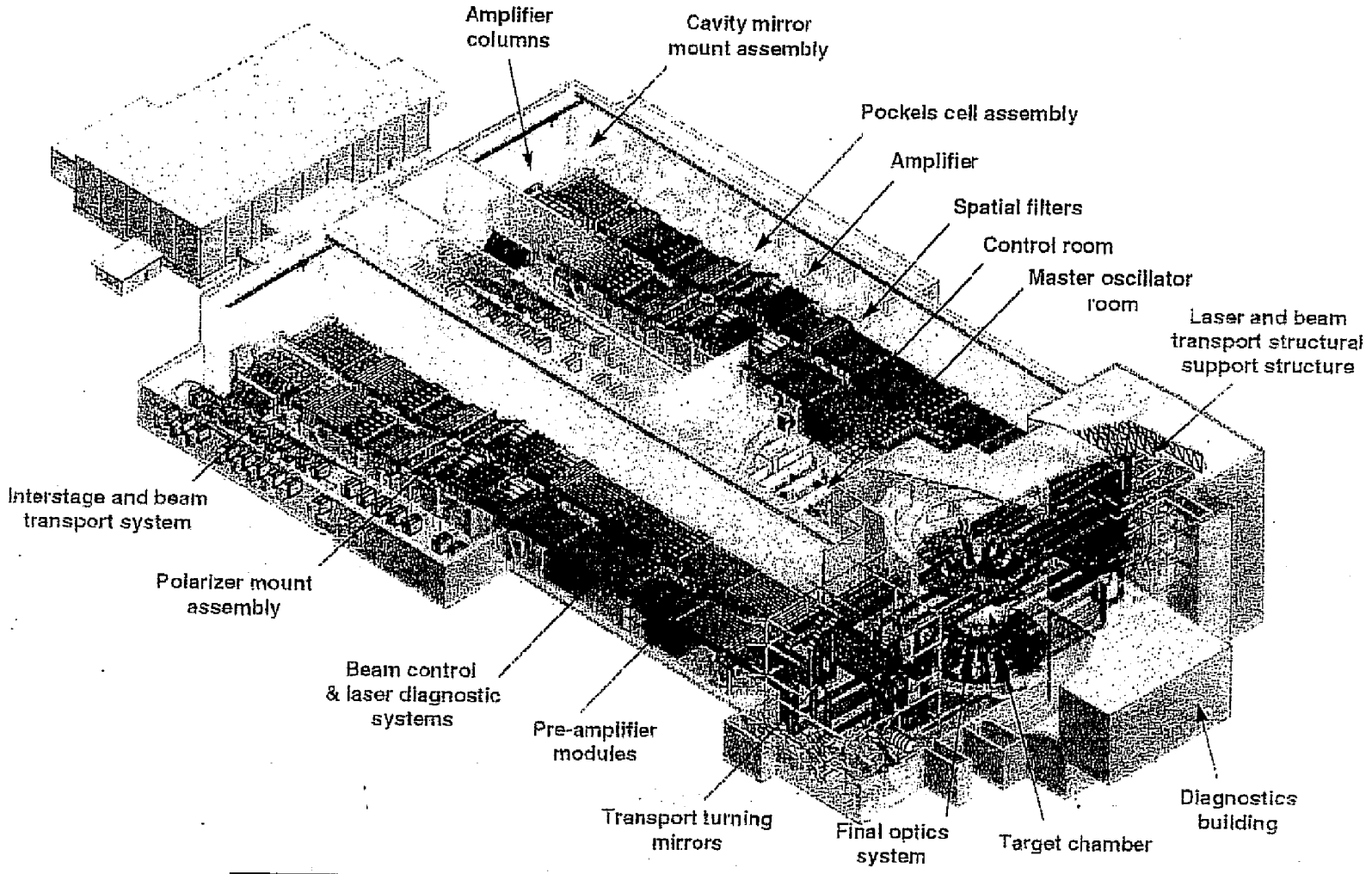

NIF illustrates many of the features of IFE development and will play a critical role in addressing IFE feasibility

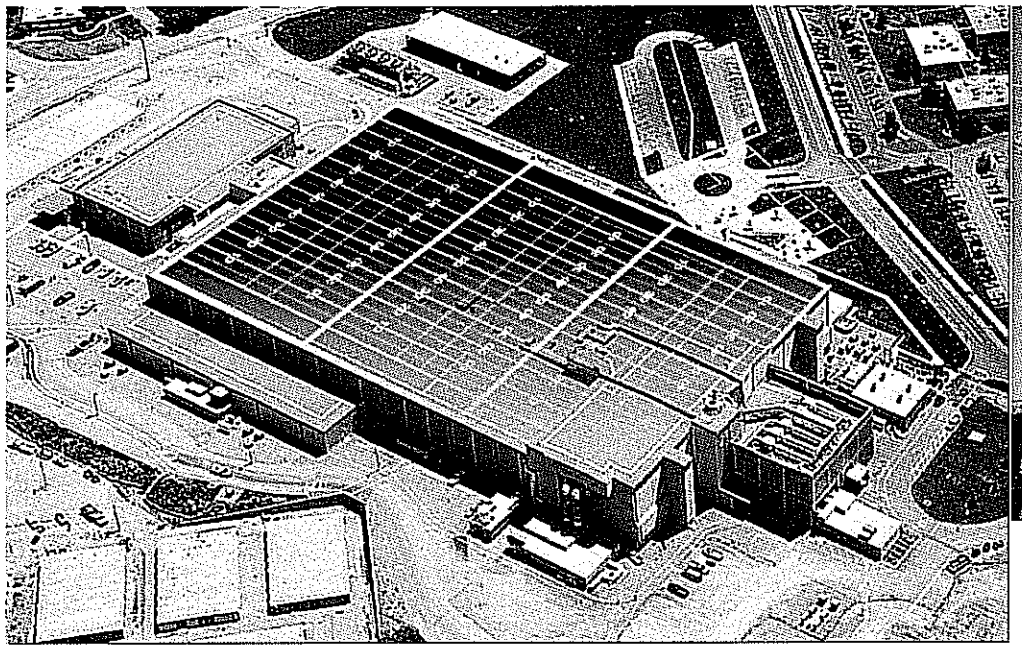

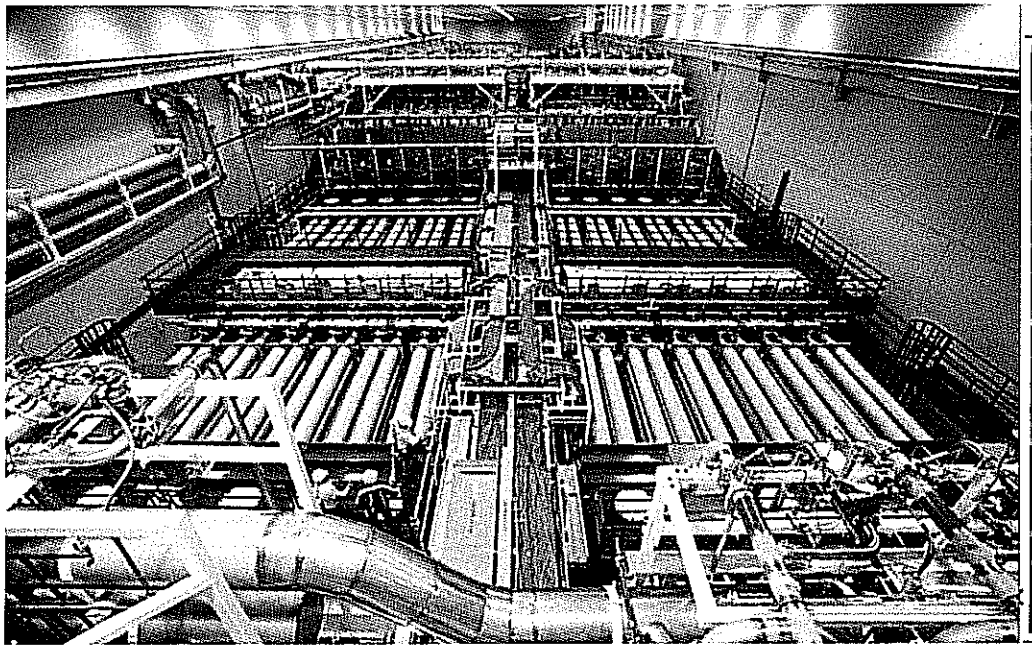

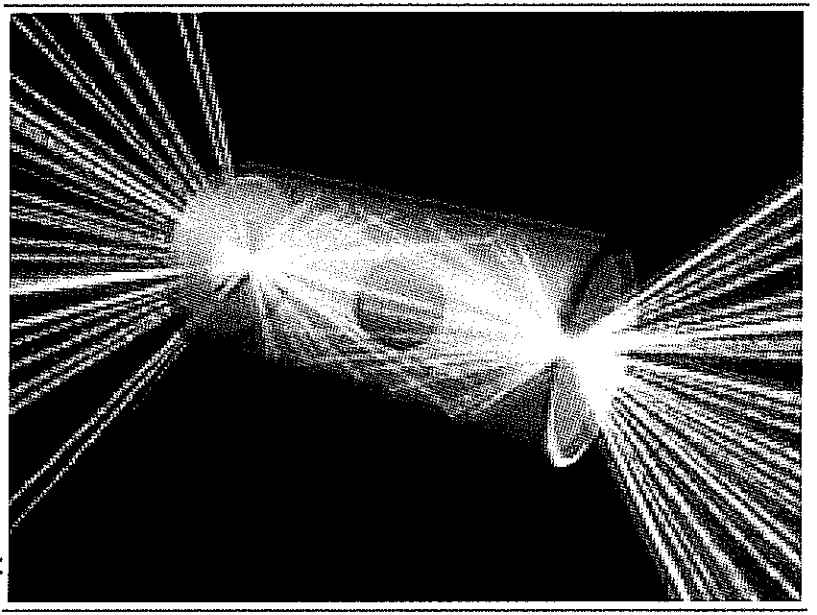

The two principal approaches to ICF are direct drive and indirect drive

Two types of targets:

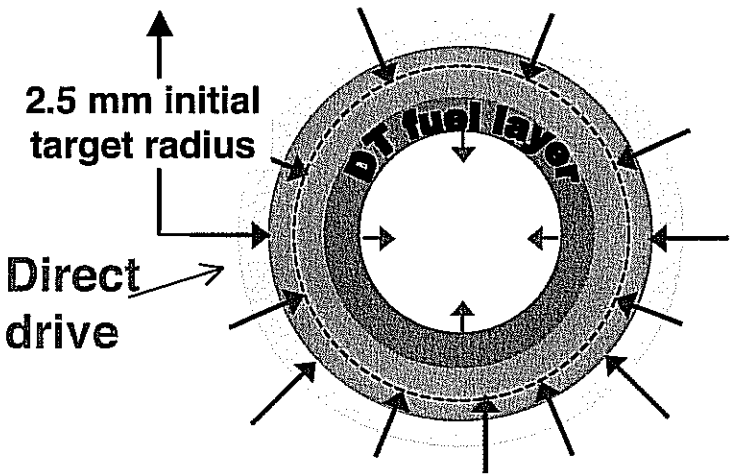

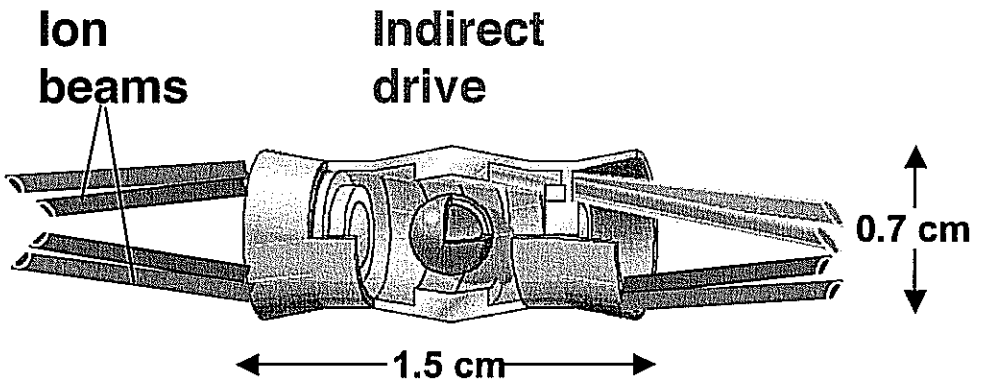

Direct drive advantages:

Higher coupling efficiency with potential for higher gain

Indirect drive advantages:

Relaxed beam uniformity (reduced hydro instability)

SIgnificant commonality for lasers and ion beams

Significant simplification of chamber geometry

The two principal approaches to ICF are direct drive and indirect drive

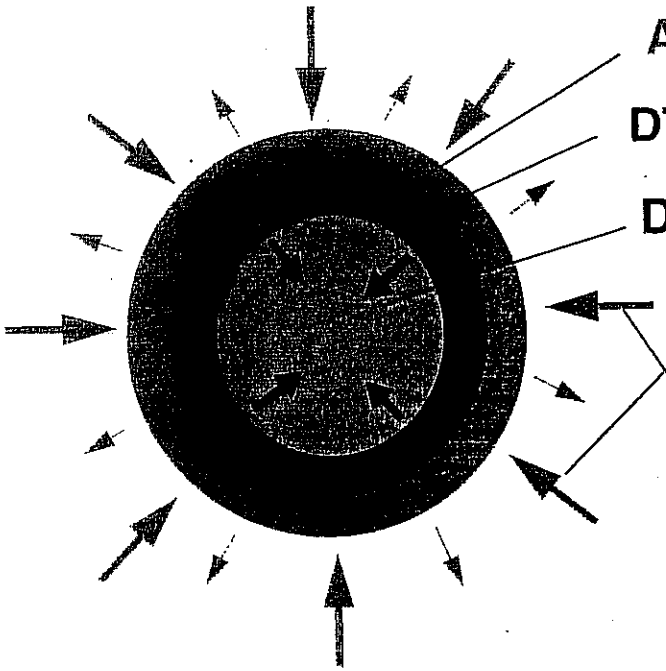

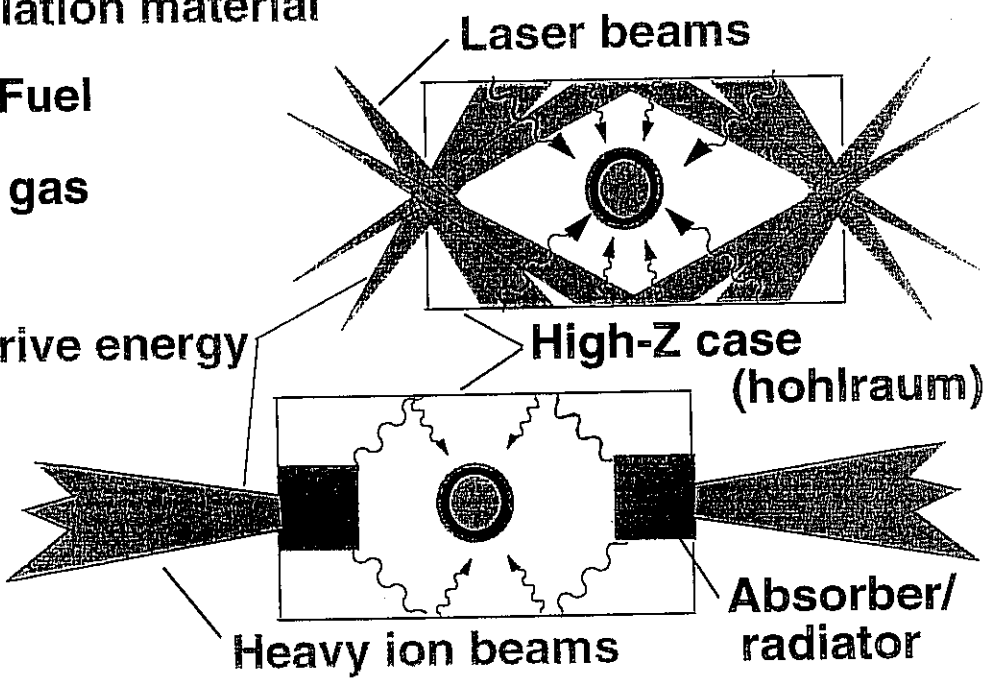

Direct drive:

Advantage:

- Higher coupling efficiency (with potential for higher gain)

Indirect drive:

Advantages:

- Relaxed beam uniformity (reduced hydro instability)
- Significant commonality for lasers and ion beams
- Significant simplification of chamber geometry

"FAST IGNITION" IS AN ALTERNATIVE TO "HOT SPOT" IGNITIO

- CAPSULE IS COMPRESSED ON LOW ADIABAT
- SECOND "IGNITER" PULSE STARTS IGNITION PROCESS

COMPRESSION PULSE $E \sim 200\,kJ - 1\,MJ$

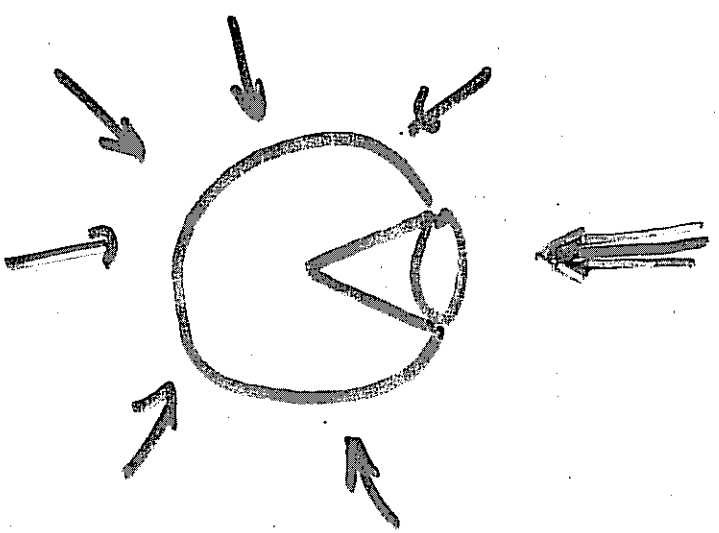

IGNITER PULSE (LIGHTER FLASHED OR ION BEAM)

$E \sim 20\,kJ$

$\tau \sim 20\,ps$

$r \sim 20\,\mu$

A "DISTRIBUTED RADIATOR" TARGET PRODUCES HIGH GAIN IN RADIATION-HYDRODYNAMIC SIMULATIONS

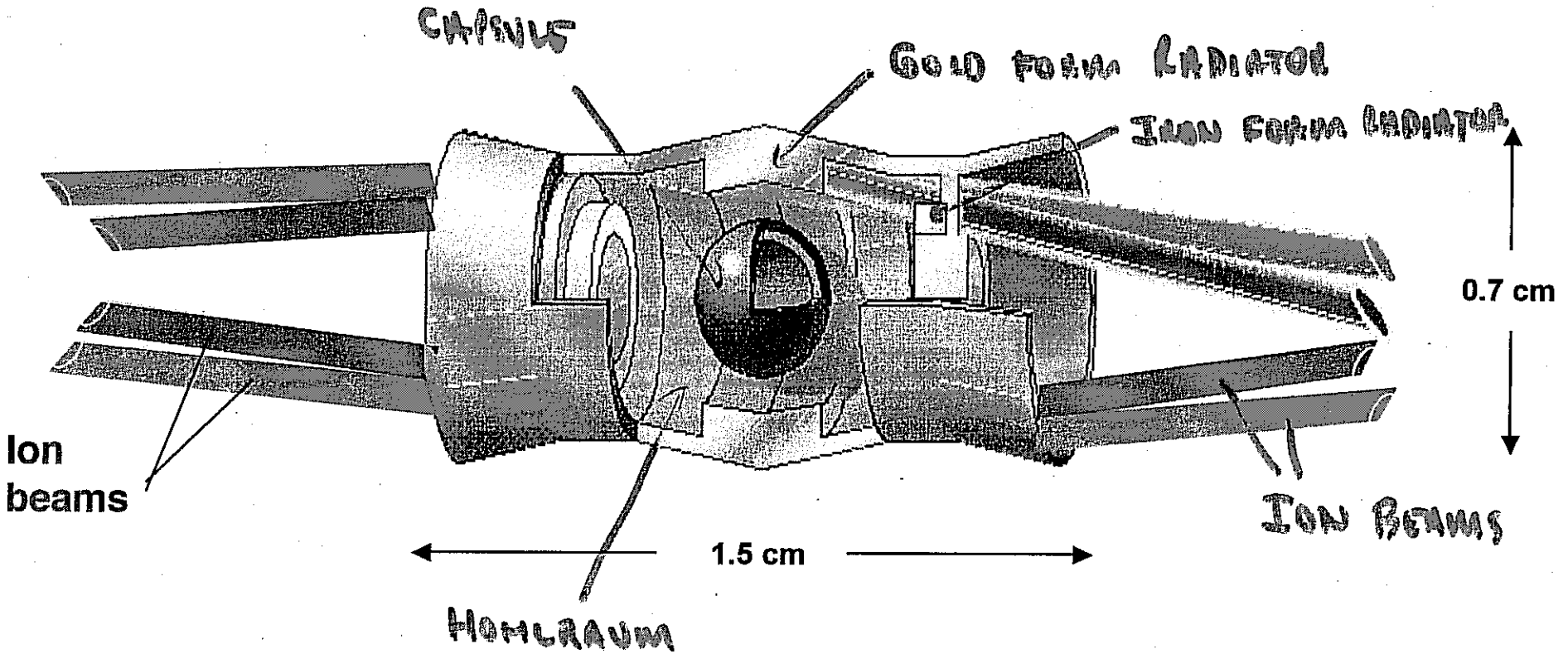

Ion current profile and radiation temperature

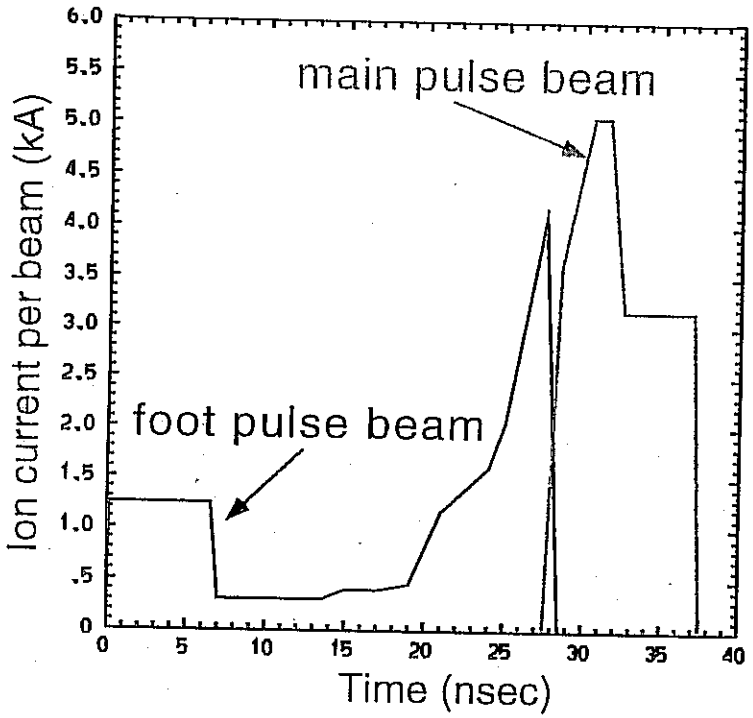

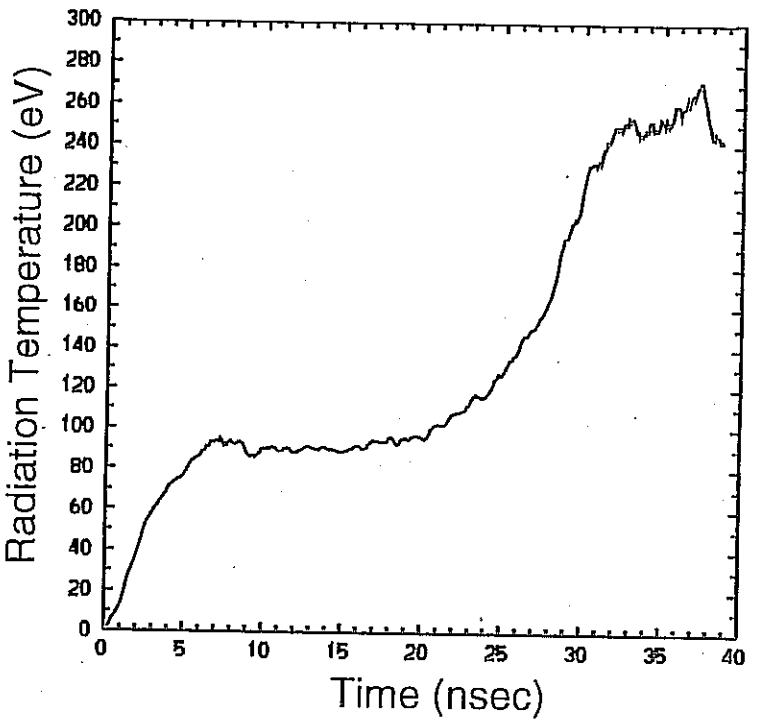

Current assumes 16 beams in foot pulse
32 beams in main pulse

Overlapping Gaussian, elliptical beams are focused at the end of the target

Each beam is an ellipse

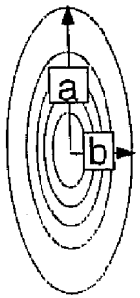

8 beams overlap in the foot pulse

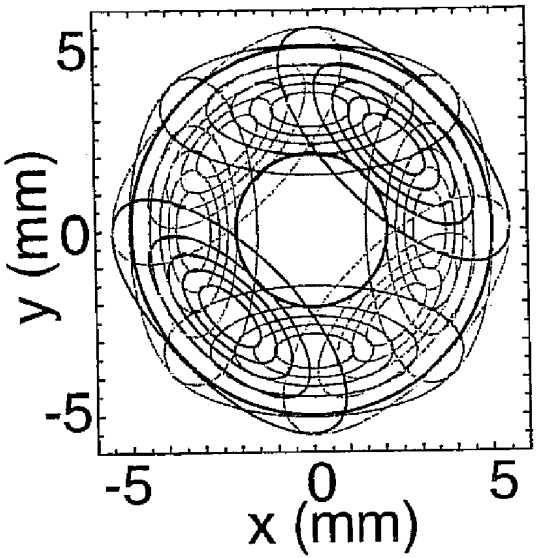

Sum of 8 foot pulse beams

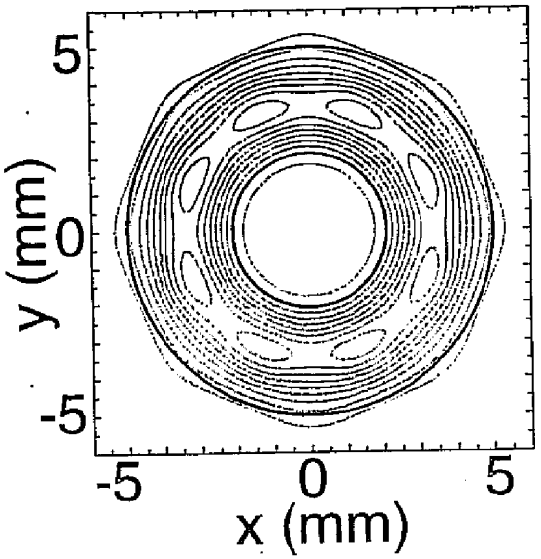

a = 4.15 mm
b = 1.8 mm
effective r=2.7 mm
95% of charge inside

Azimuthal asymmetry:
foot pulse: -1.6% in m=8
main pulse: 0.06% in m=16

Callahan 8/97

Why Heavy Ions?

Target requires:

3.5 - 6 MJ in ~ 10 ns $\Rightarrow$ ~ 500 TW

Range ~ 0.02 - .2 g/cm^2

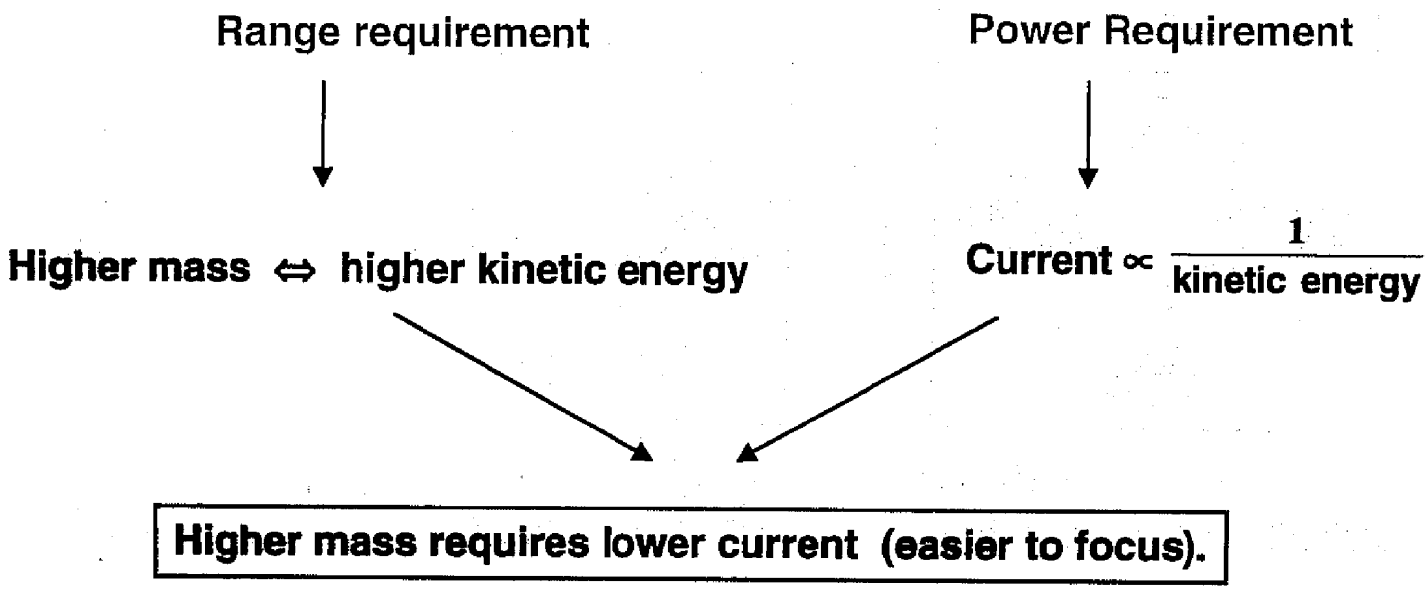

(5)

Heavier Ions ⇒ Higher Kinetic Energy

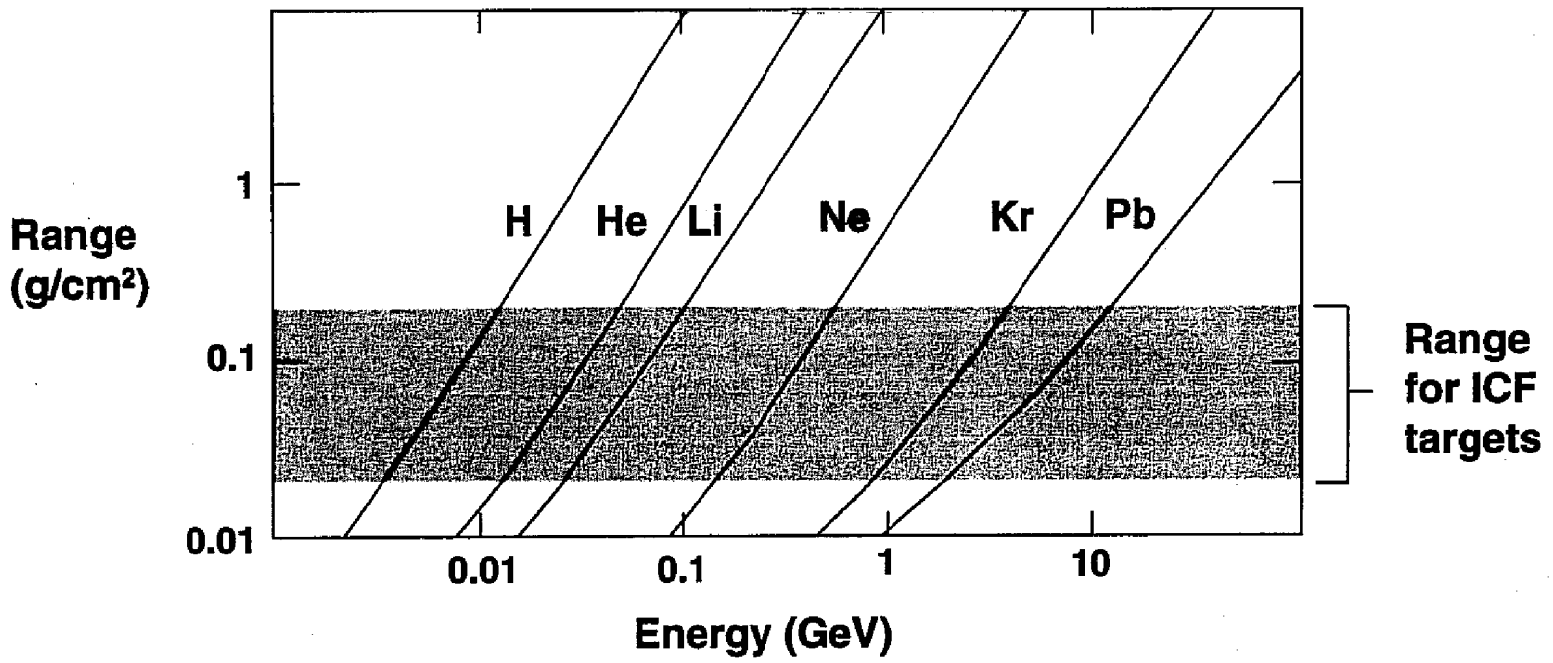

Targets require high power (kinetic energy x current).

- **Light Ion Fusion requires high-current, unconventional accelerators (Sandia 1970s).**
- **Heavy Ion Fusion requires lower currents enabling the use of more conventional high energy accelerators (Maschke ~ 1974).**

There are two principle methods of acceleration

1. r.f. acceleration

(Approach in Europe and Japan)

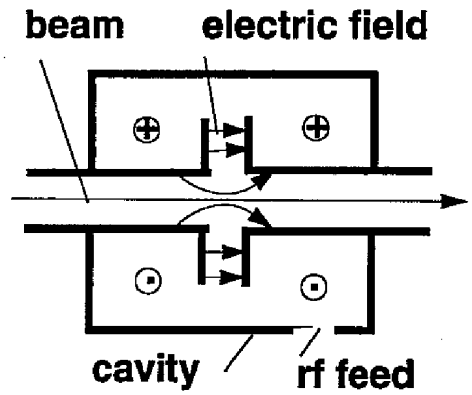

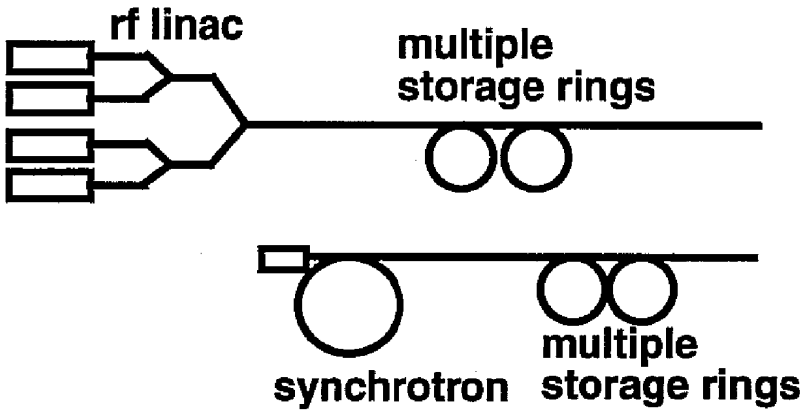

2. Induction acceleration

(U.S. approach)

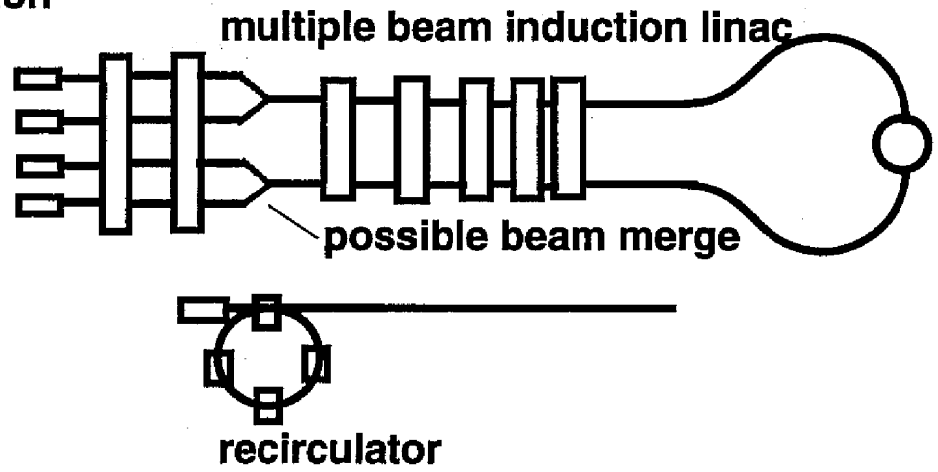

Induction acceleration for HIF consists of several subsystems and a variety of beam manipulations

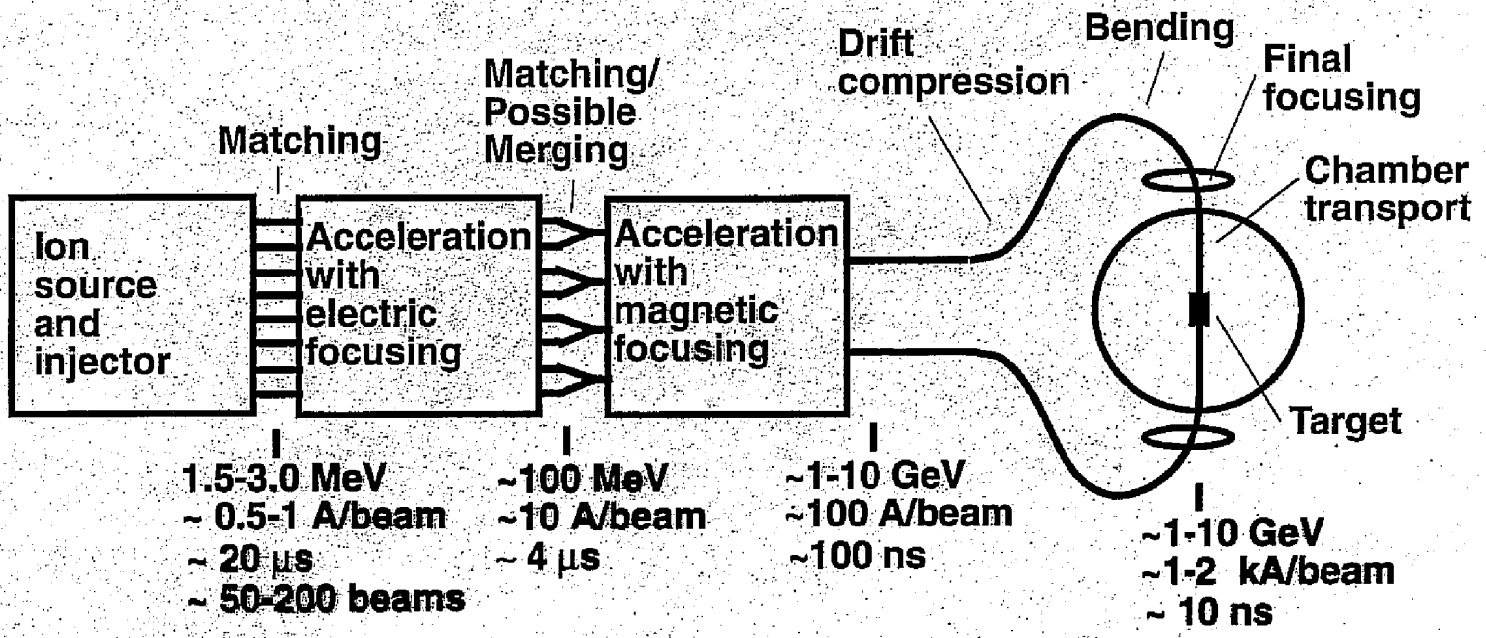

A Robust Point Design study established a baseline for a multiple-beam quadrupole induction linac HIF driver

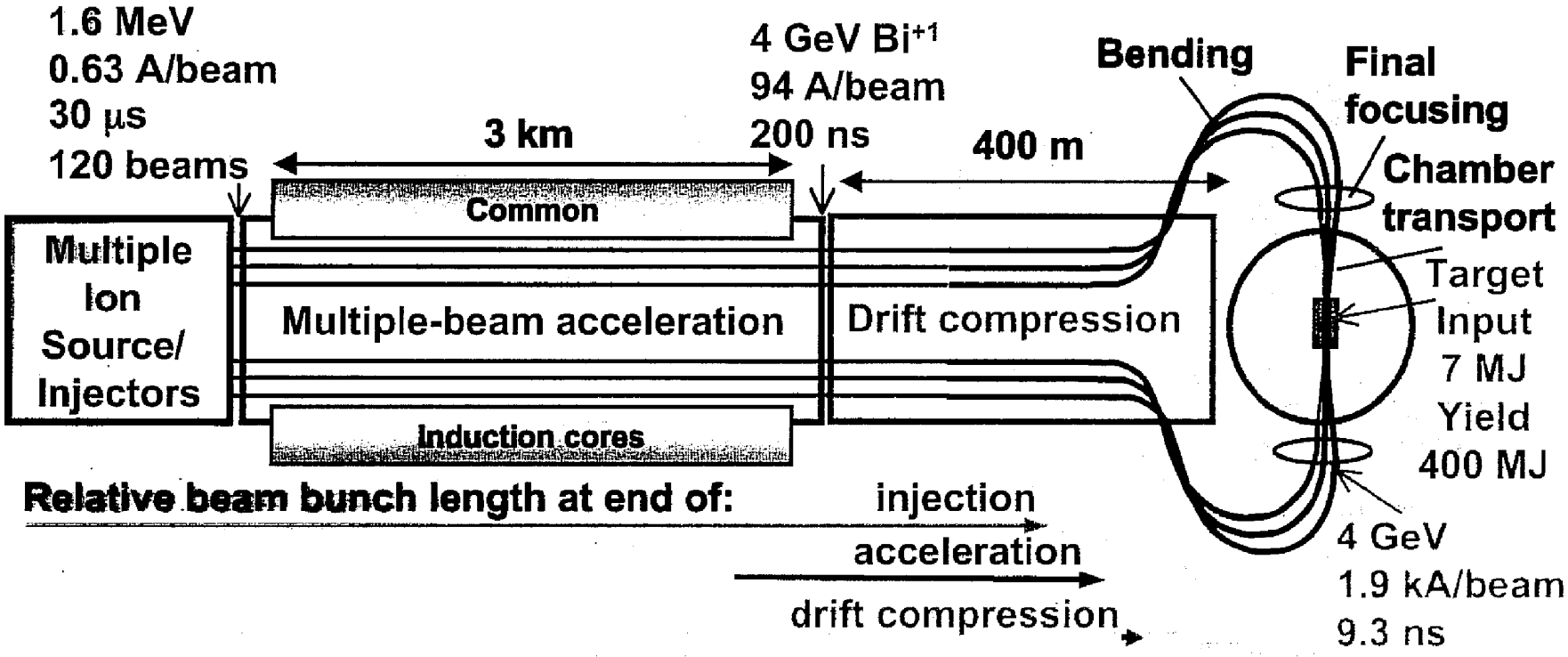

A solenoid focus option leads to a low V, high current modular driver with advantageous development path

Pulse energy ~ 6.7 MJ

V~ 200-300 MV: T~ 2.5 GeV Xe^{+8} ions or T ~ 200 MeV for Ne^{+1}

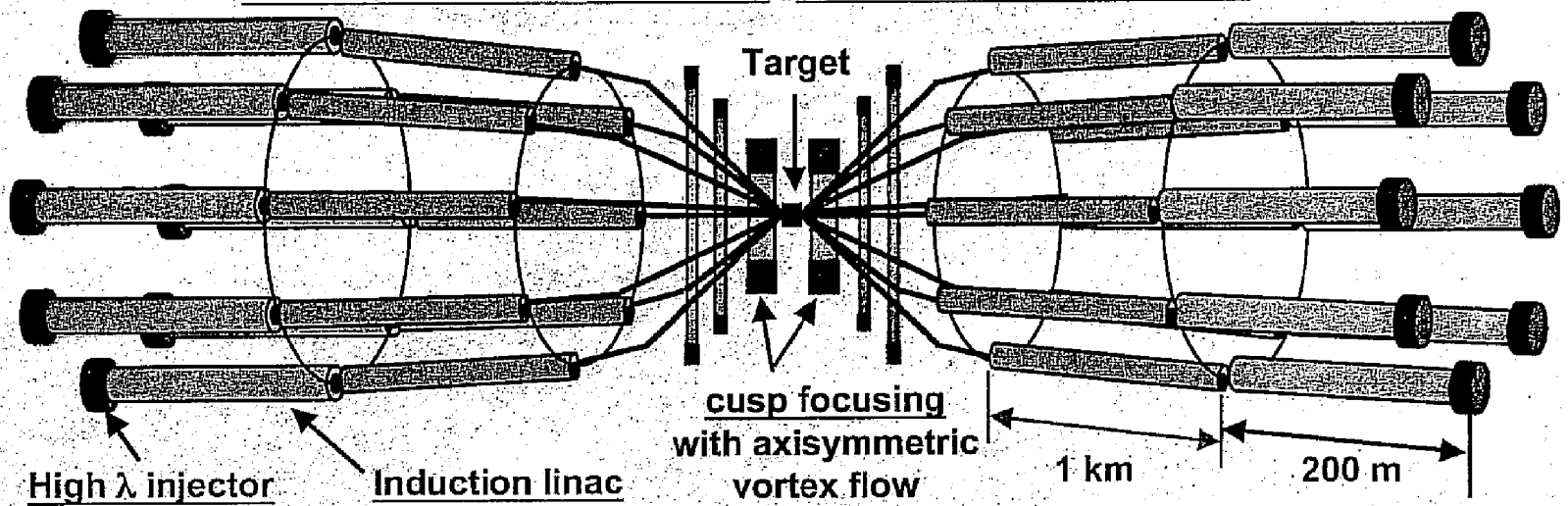

High λ injector

Merging beamlet source/injector

or

accel/decel injector

Induction linac

single beams

r_p ~ 15 cm

B_s ~ 9T

I ~ 6.7 kA

T ~ 2.5 GeV

Δt ~ 100 ns

double pulsed for foot and main pulses

or

adiabatic plasma lense assisted pinch with cross-jet flow. liquid walls

Neutralized drift compression

Δv/v ~ 0.01

(no space charge stagnation)

Summary of Current Limits From Different Focusing Methods

Einzel Lens

$$Q_{max} \cong \frac{3\pi^2}{\gamma}\left(\frac{q\phi_0}{m v_0^2}\right)^2\left(\frac{r_b}{L}\right)^2$$

Solenoids

$$Q_{max} = \left(\frac{\omega_c r_b}{2\gamma\beta c}\right)^2$$

Quadrupole Focusing

$$Q_{max} \cong \frac{\eta\sigma_0}{2\pi}\left(\frac{\sin\frac{\eta\pi}{2}}{\frac{\eta\pi}{2}}\right)\left[\frac{Br_b}{[B\rho]}\left[\frac{r_b}{r_p}\right]\right.$$ (Magnetic)

$$\left.\frac{2qV_q}{\gamma m v_z^2}\left[\frac{r_b^2}{r_p^2}\right]\right]$$ (Electric)

For Non-Relativistic Beams

$$\lambda_{max} \propto \frac{\phi_0^2}{V}$$

$$\lambda_{max} \propto \frac{q}{m} B^2 r_p^2$$

$$\lambda_{max} \propto \begin{cases} B_\perp V^{1/2} r_p \\ V_q \end{cases}$$

Note
- ϕ_0 = Voltage between Einzel lenses
- V_q = Voltage on a quad relative to ground
- V = particle energy / q

Major components of an induction linac

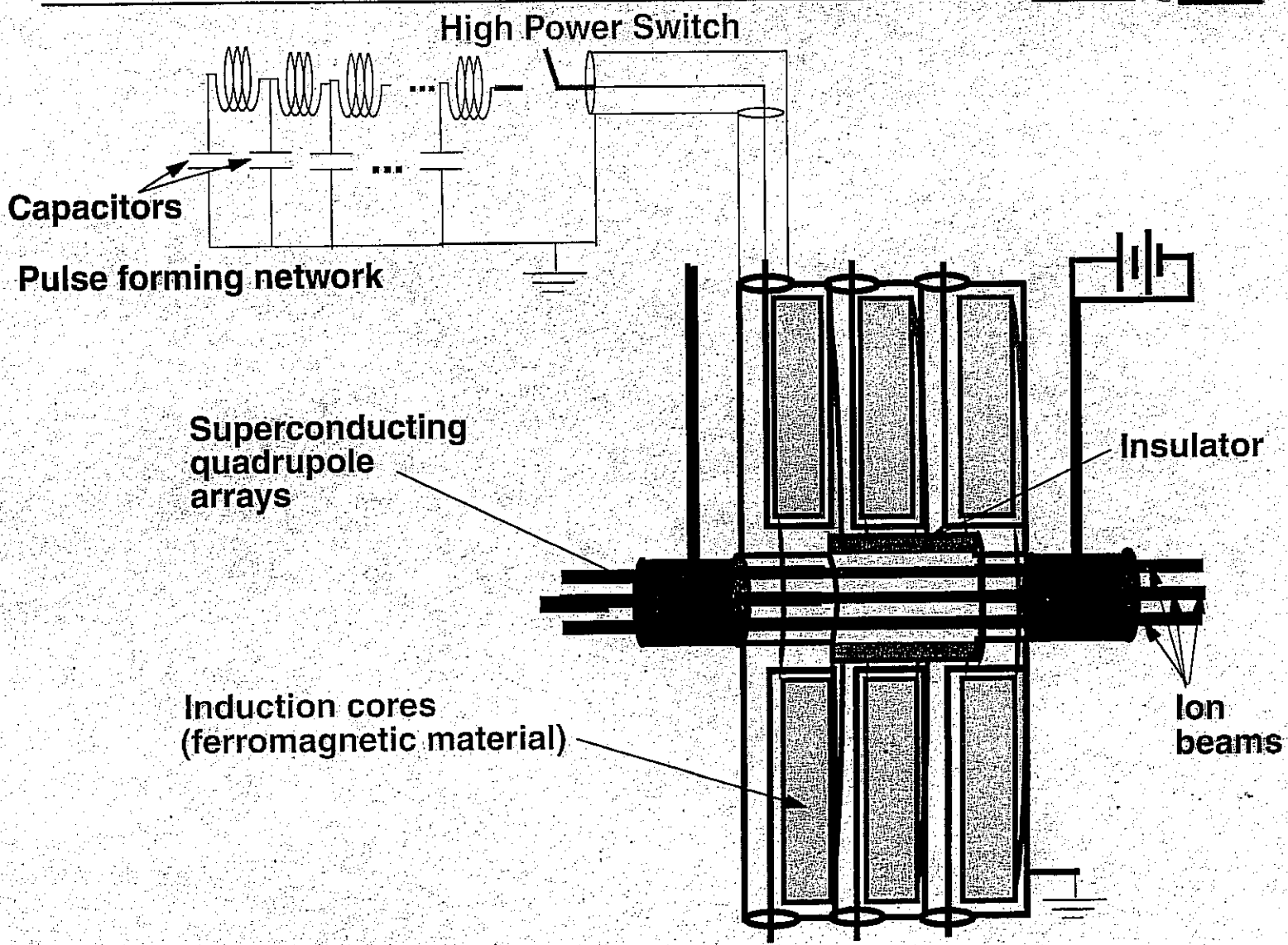

An Induction Core

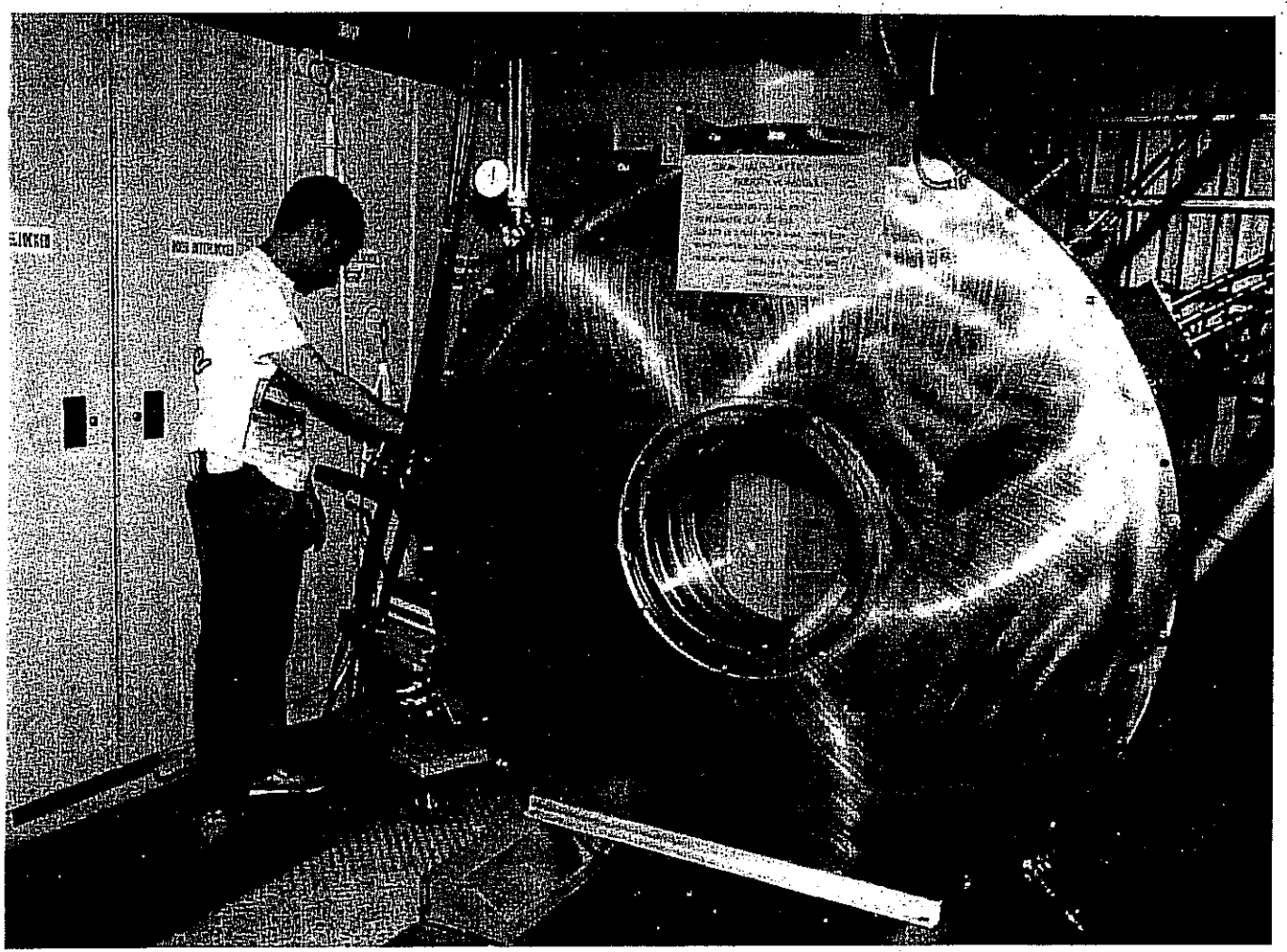

An array of small beamlets increases the total beam current through the core

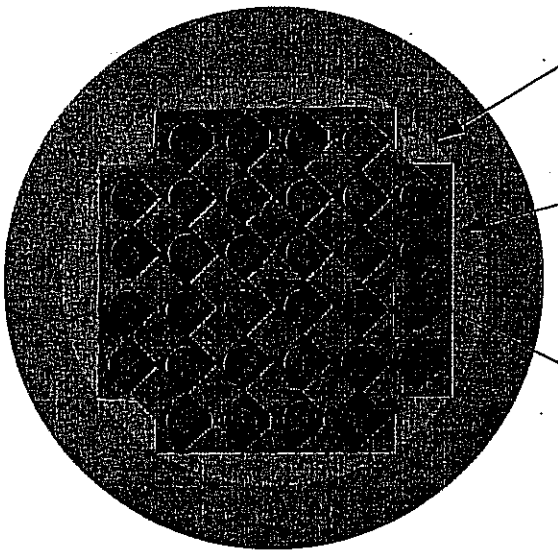

Core (radius = R_{core})

Multibeam quad array

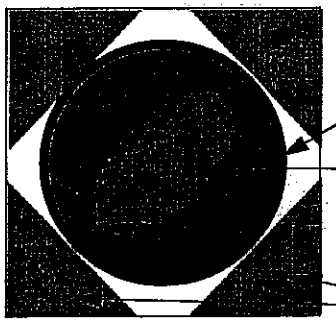

beam pipe (radius = r_p)

beam (radius = a)

quadrupole magnet winding

From class:

$$\frac{Q}{a} = \left(\frac{\sigma_0^2}{4L^2}\right)\sigma_0$$

$$\sigma_0 \cong \frac{\eta L^2}{[B\rho]}\frac{B'}{[B\rho]}$$

$$Q \simeq \frac{\eta B' \sigma_0}{[B\rho]}\frac{a}{4}$$

$$I \sim \rho^3 Q \sim a^2 B \beta^2 / r_p$$

Current per beam = $I_b \sim a^2 B \beta^2/r_p$

$r_p \sim a$ (until misalignments require minimum size--better: $r_p = c_1 a + c_2$)

so $I_b \sim a$; N_b = number of beams in array $\sim R^2_{core} / a^2$

Total current through core = $I_{tot} = N_b I_b \sim R^2_{core} / a$ (until misalignments dominate scaling)

A Typical driver has about 2000 individual modules

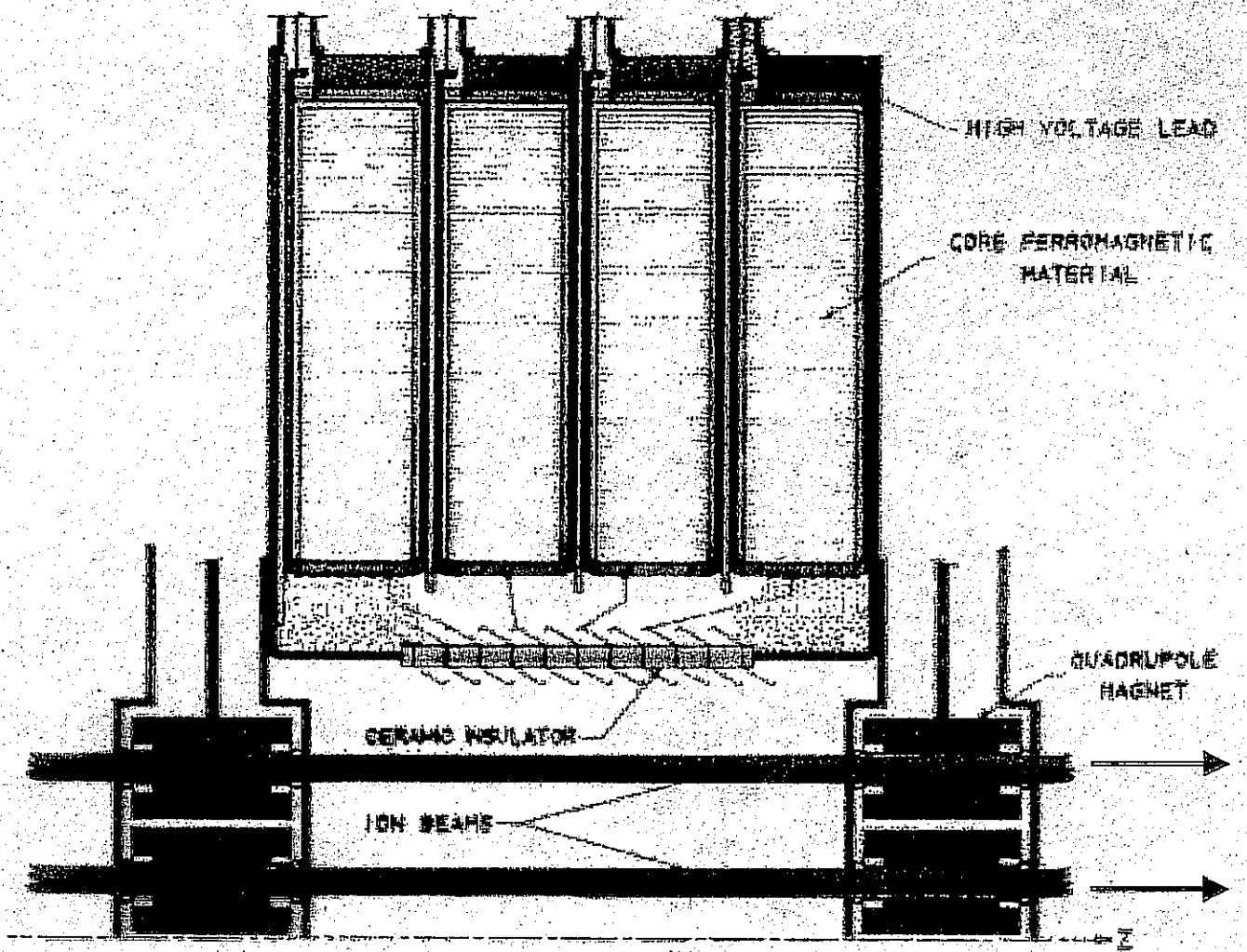

Focusability at the target is key scientific issue

Conditions of beam at target are set by hohlraum and implosion physics

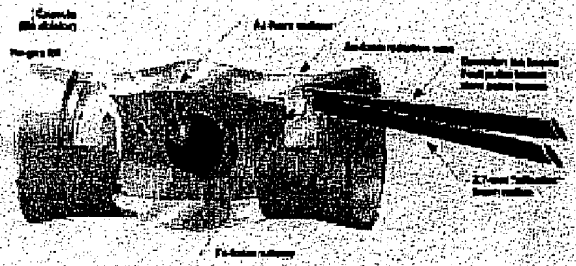

Energy in pulse: ~ 3 to 6 MJ

Duration of main pulse: ~ 8 to 10 ns

Duration of foot pulse: ~ 30 ns

Spot radius: ~ 1.5 to 3 mm

Transverse and longitudinal compression are required to meet target specifications.

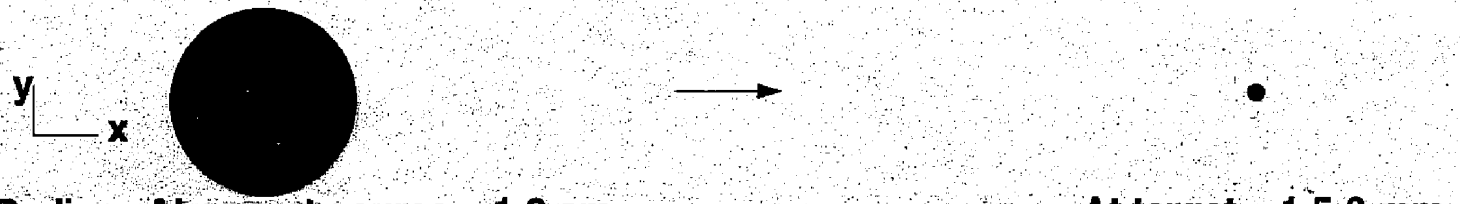

Compression factors of 10 to 50 in both longitudinal and transverse directions are required.

In an induction linac, certain limits constrain design

Phase advance per lattice period $\sigma_0 < \sim 85^o$ **(to avoid envelope/lattice instabilities & emittance growth).**

Space charge is limited by external focusing $K < (\sigma_0 a/2L)^2$ **where K is the perveance (proportional to line charge density over beam Voltage), a is the average beam radius and L is the half-lattice period.**

Velocity tilt $\Delta v/v < \sim$ 0.3 for electrostatic quads **(larger for magnetic quads) to avoid mismatches at head and tail of beam, and to ensure tail radius within pipe and head σ_0 within limit)**

Volt-seconds per meter $(dV/ds)\, l/v_0 <\sim$ 1.5-2.0 V-s/m **(for "reasonable" core sizes)**

Voltage gradient dV/ds < ~ 1-2 MV/m **(to avoid breakdown in gaps)**

Sources of non-linearity and mismatch are well defined

Sources of non-linearities

- External focusing magnets
- Space-charge
- Multiple-beam effects

Sources of mismatch

- Accelerator imperfections
  - Quad strength and placement errors
  - Acceleration waveform errors
  - Bend strength errors
- Velocity tilt

Simulations give reliable and definitive tolerances on each source

Several potential instabilities have been investigated in HIF drivers

Temperature anisotropy instability

After acceleration $T_{||} << T_{\perp}$, internal beam modes are unstable; saturation occurs when $T_{||} \sim T_{\perp}/3$

Longitudinal resistive instability

Module impedance interacts with beam, amplifying space-charge waves that are backward propagating in beam frame

Beam break-up (BBU) instability

High frequency waves in induction module cavities interact transversely with beam

Beam-plasma instability

Beam interacts with residual gas in target chamber

All of these instabilities have known analytic linear growth rates, which constrain the accelerator design (to ensure minimal growth or benign saturation).

M. de Hoon studied a final current pulse that is flat with parabolic ends using the HERMES code

15 ns final pulse duration

The initial tilt on the beam is about 4% (compare to ~30% at the beginning of the accelerator)

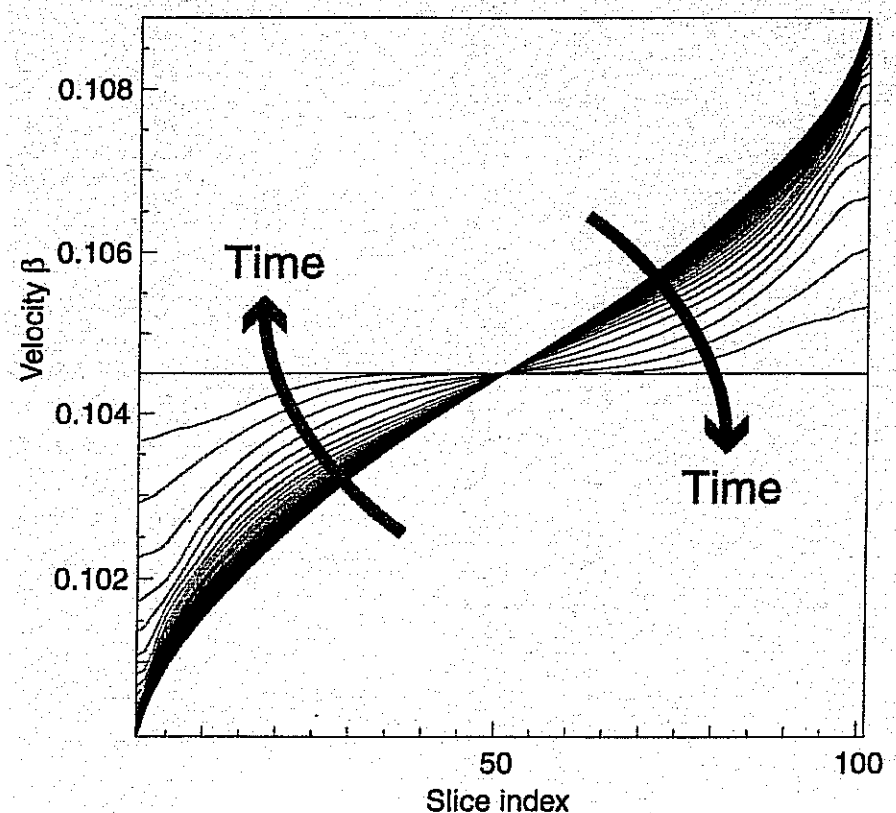

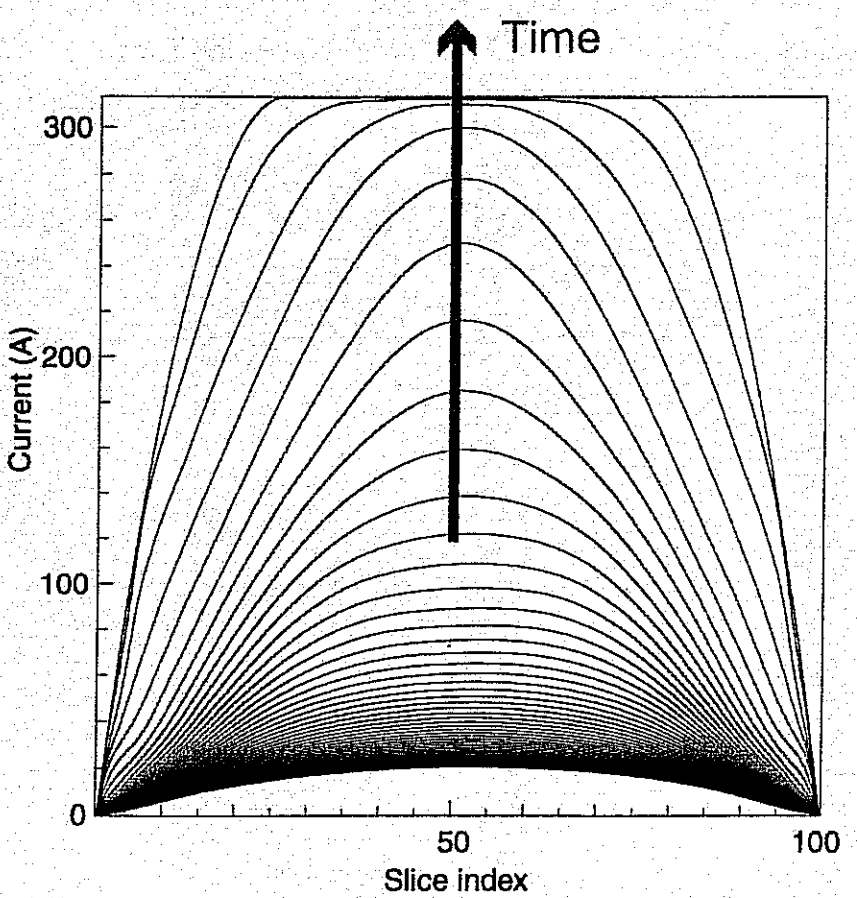

Although the final beam profile is flat, it is parabolic for most of the drift compression

Drift compression section is designed by running code first backwards from target, then forwards after rematching

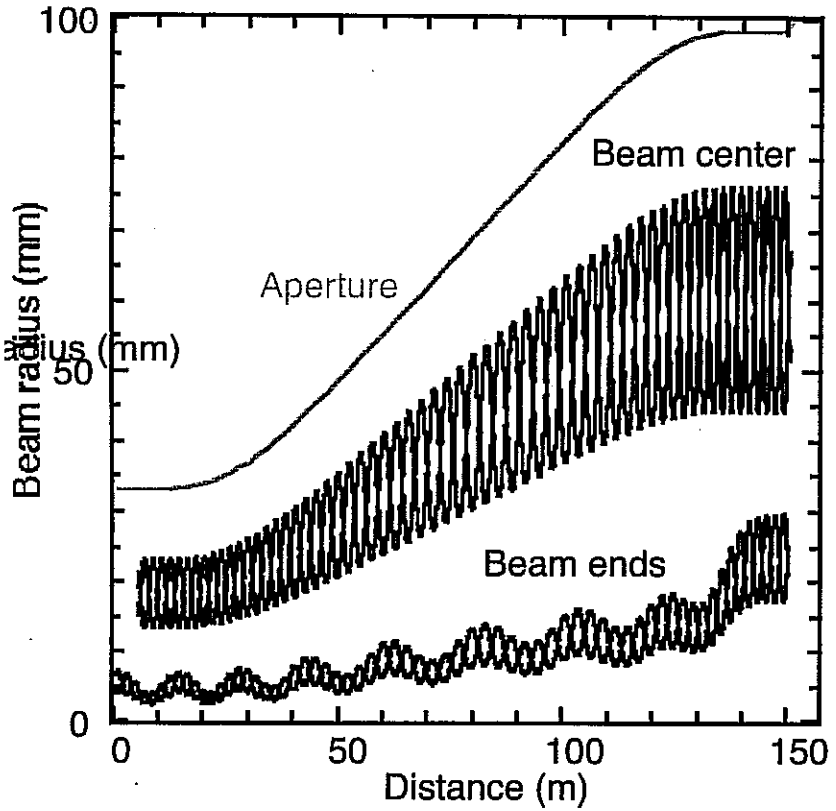

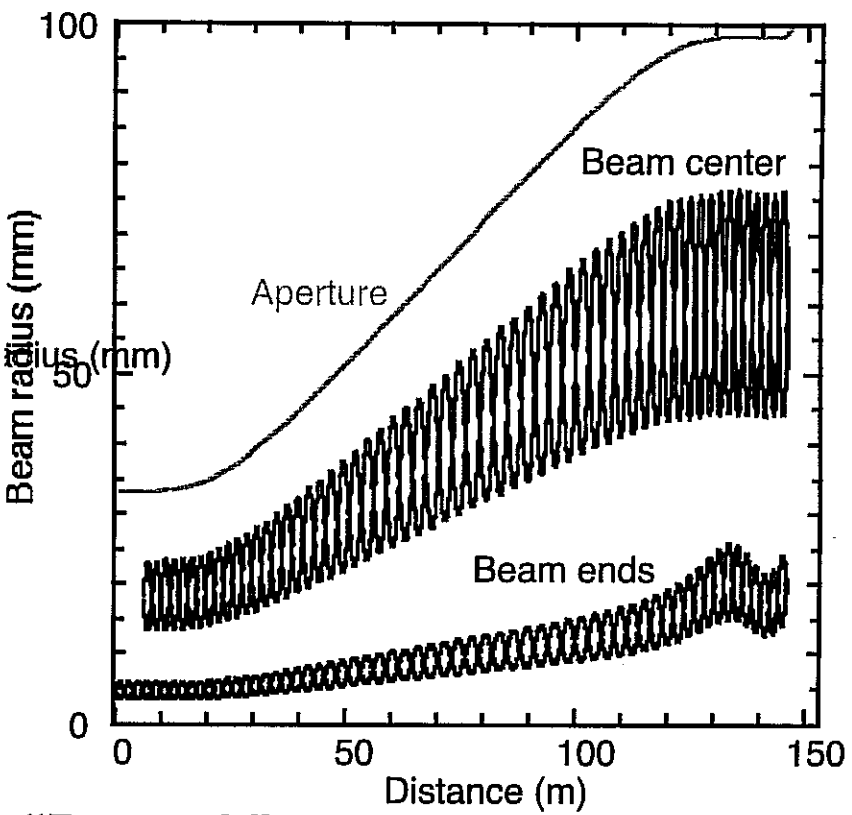

Begin with a desired 20ns, constant-energy pulse at end of compression, track backwards, design lattice for central slice; beam end becomes mismatched early on

"Rematch" at entrance to compression section, by adjusting a,a',b,b'; then track forward

The HYLIFE-II Ion beam-driven power plant is shown with a two-end target, illustrated from two sides and a linear heavy-ion induction driver

The liquid wall protection including beam ports is provided by pumping molten salt (Flibe) through the chamber

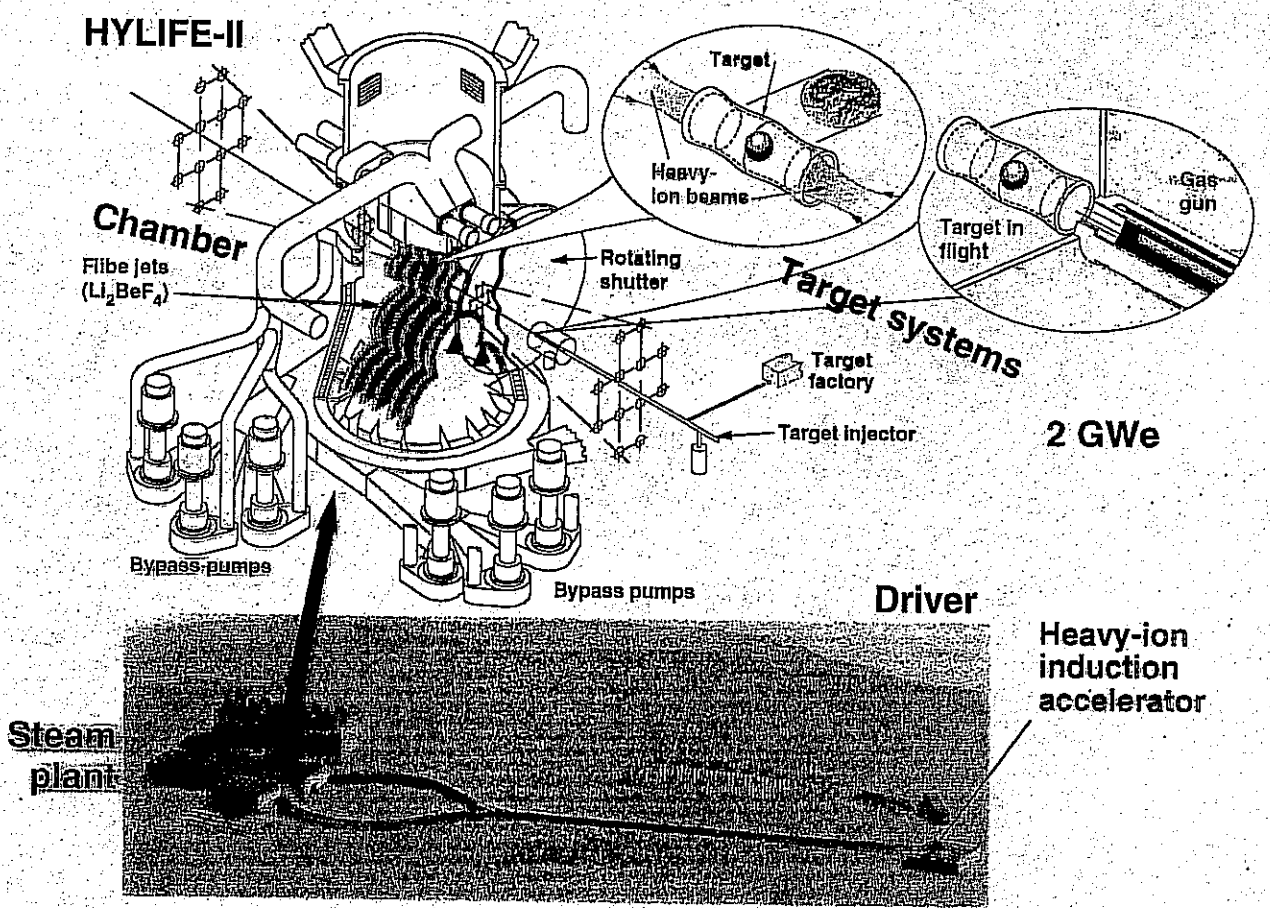

Liquid-jet protected fusion chambers for long lifetime, low cost, and low environmental impact

The First Wall Protected by Neutron-thick Molten Salt FLiBe,

FLiBe is a low Z salt ⇒ low activation ⇒ Green fusion energy

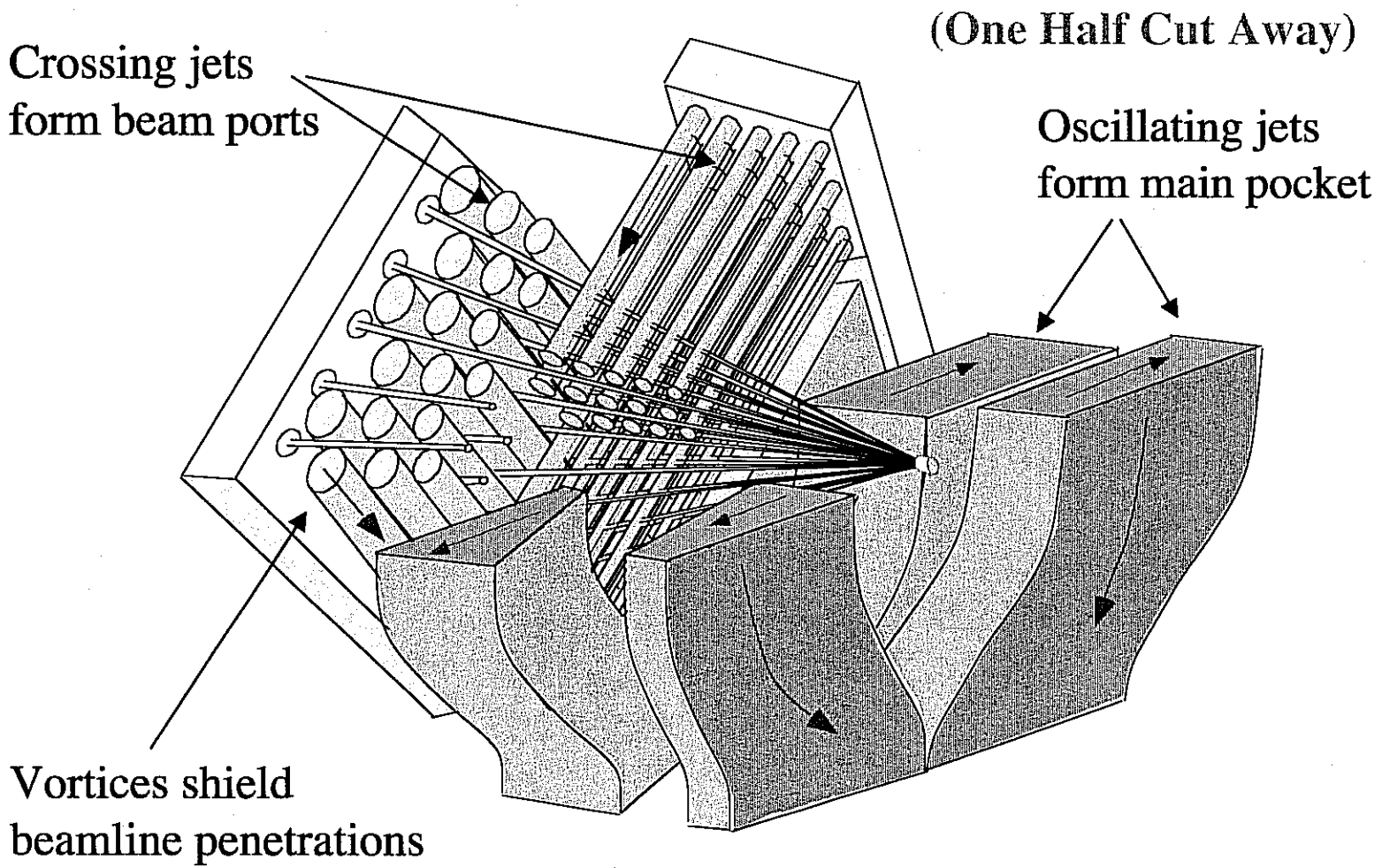

A number of final focus options are being considered for HIF applications

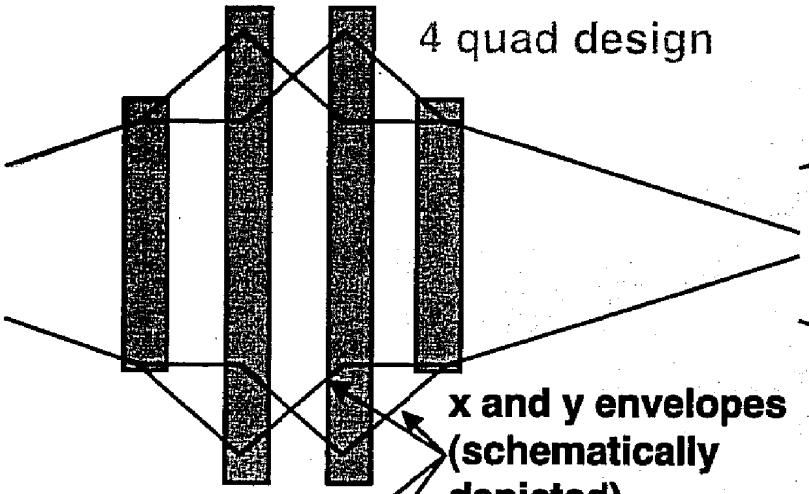

x and y envelopes (schematically depicted)

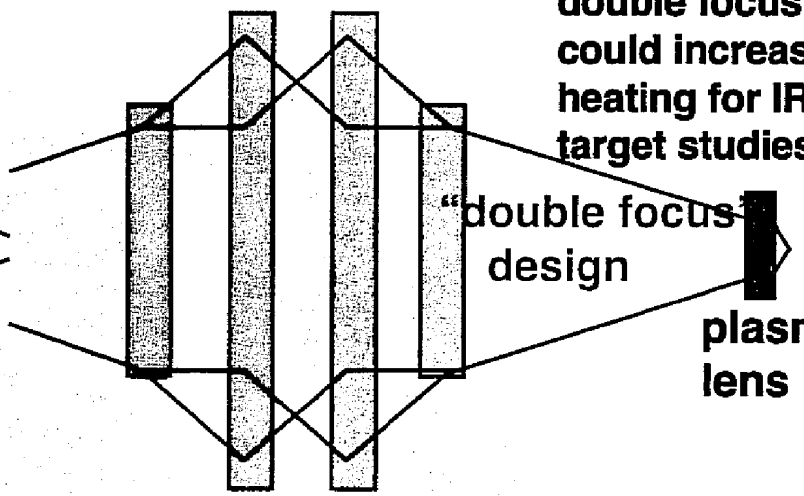

double focus design could increase spot heating for IRE target studies

plasma lens

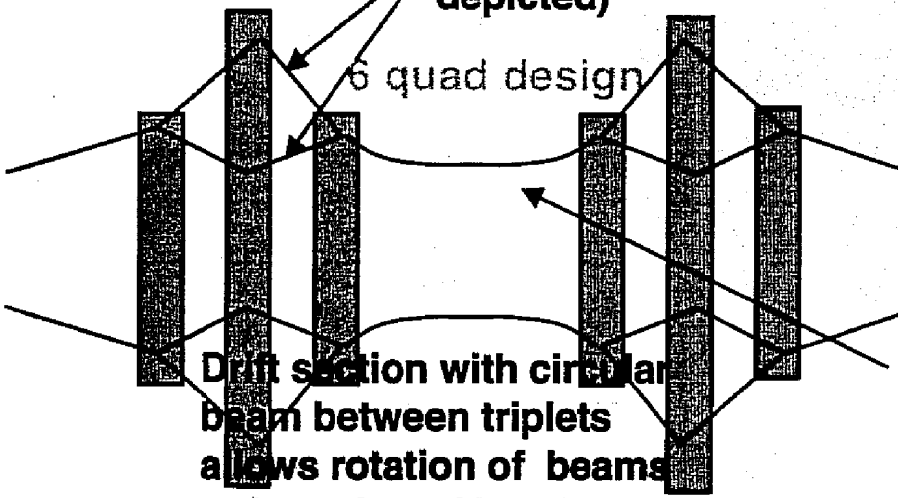

Drift section with circular beam between triplets allows rotation of beams or insertion of bend

Solenoid or cusp focusing is being considered for modular drivers:

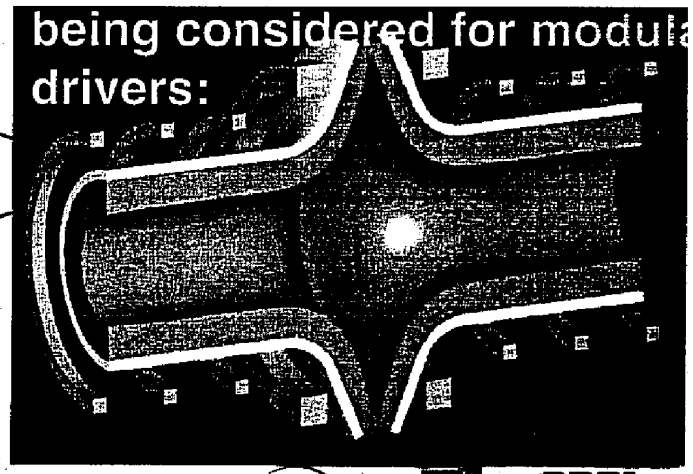

ESTIMATING SPOT SIZE

$$r_x'' + \frac{(\gamma_b \beta_b)'}{\gamma_b \beta_b} r_x' + \kappa_x r_x - \frac{2Q}{r_x + r_y} - \frac{\varepsilon_x^2}{r_x^3} = 0$$

$$r_y'' + \frac{(\gamma_b \beta_b)'}{\gamma_b \beta_b} r_y' + \kappa_y r_y - \frac{2Q}{r_x + r_y} - \frac{\varepsilon_y^2}{r_y^3} = 0$$

IN CHAMBER: NO EXTERNAL FOCUSING, NO ACCELERATION AND BEAM IS OFTEN CIRCULAR (BY DESIGN)

$$\Rightarrow \kappa_x = \kappa_y = (\gamma_b \beta_b)' = 0 \quad \& \quad r_x = r_y = r_b$$

$\Rightarrow$ ENVELOPE EQUATION IS:

$$r_b'' = \frac{Q}{r_b} + \frac{\varepsilon^2}{r_b^3}$$

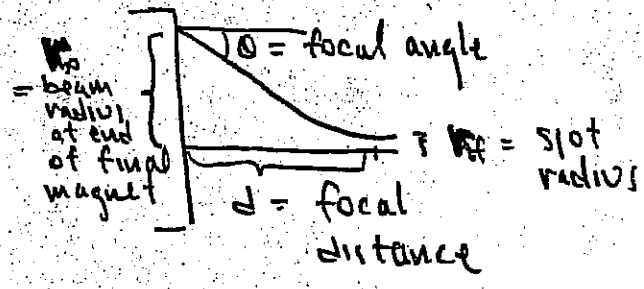

MULTIPLYING BY r_b' & INTEGRATING $\Rightarrow$

$$\frac{r_{bf}'^2}{2} - \frac{r_{b0}'^2}{2} = Q \ln \frac{r_{bf}}{r_{b0}} + \frac{\varepsilon^2}{2 r_{b0}^2} - \frac{\varepsilon^2}{2 r_{bf}^2}$$

NOW $r_{b\theta}' \cong \theta$ $\quad r_{bf}$ = spot radius $\quad r_{bf} \ll r_{b0}$

$r_{bf}' = 0$ $\quad r_{b0} \cong d\theta$

$$\Rightarrow \boxed{\theta^2 \cong 2Q \ln\left(\frac{\theta d}{r_{bf}}\right) + \frac{\varepsilon^2}{r_{bf}^2}}$$

FOR EMITTANCE DOMINATED SPOT: $r_{bf} = \frac{\varepsilon}{\theta}$

"CHROMATIC ABERRATIONS" TEND TO BROADEN SPOT

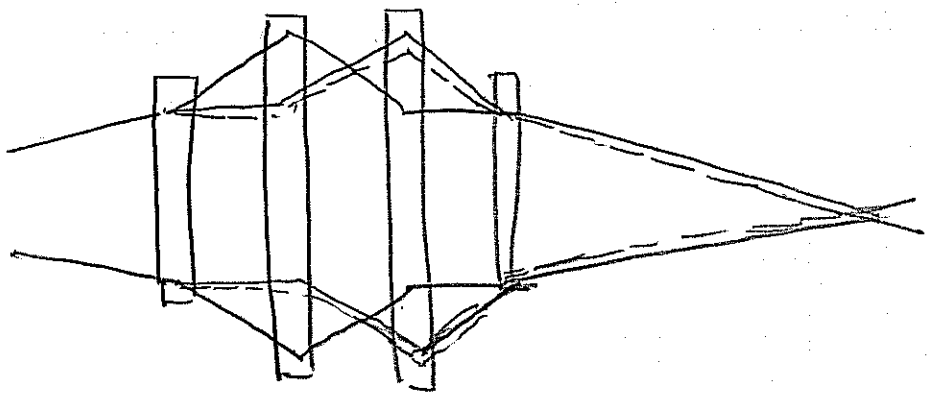

SINCE QUADRUPOLE MAGNET FOCUSING $\propto \frac{1}{V_z}$

(i.e. $x'' = \frac{qB'}{\gamma m v_z} x$) A SPREAD IN LONGITUDINAL VELOCITY GIVES RISE TO A BROADENING OF FINAL SPOT.

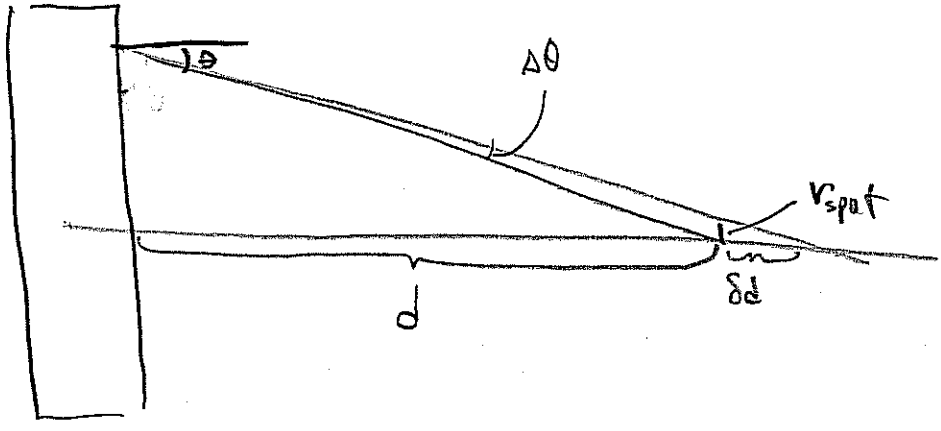

$$r_{spot} = \theta \delta_d$$

$$= \theta \frac{\partial d}{\partial \theta} \frac{\partial \theta}{\partial \gamma} \delta_\gamma$$

$$= \alpha \theta d \left(\frac{\delta_p}{p}\right)$$

α = some constant depending on focal system

HEURISTICALLY THE CONTRIBUTION FROM CHROMATIC ABERRATIONS CAN BE WRITTEN

$$\nu_{chrom}^2 = \alpha^2 \mathcal{D}^2 \left(\frac{\delta\gamma}{\gamma}\right)^2 \theta^2$$

where α depends on system, typically 4-8

$$\nu_{spot}^2 = \nu_{bf}^2 + \nu_{chrom}^2$$

DETAILED SIMULATIONS OR MOMENT CODE RESULTS REQUIRED TO FIX α.

We constructed moment models to study chromatic effects (through 2nd order) in final focus system

$$\frac{dp_x}{dt} = q(E_x + v_z B_y - v_y B_z)$$

Expand through 2nd order in x', y', $k_{\beta 0}x$, $k_{\beta 0}y$, $\delta p/p$

$$x'' + \left(\frac{1}{\gamma v_{z0}}\frac{d}{dz}(\gamma v_z)\right)x' = \frac{qB'}{\gamma m v_{z0}}x\left(1 - \frac{\delta p}{p}\right) + \frac{q\lambda}{4\pi\varepsilon_0 m v_{z0}^2}\frac{(x-\bar{x})(1-\frac{2\delta p}{p})}{(\Delta x^2 + [\Delta x^2 \Delta y^2]^{1/2})}$$

The equation of motions can be written (where $\delta = \delta p/p$) :

$$x'' = K_{xx}x + K_{xx1}x\delta \qquad y'' = K_{yy}y + K_{yy1}y\delta$$

Here:

$$K_{xx} = \frac{B'}{[B\rho]_0} + \frac{Q}{2(\Delta x^2 + [\Delta x^2 \Delta y^2]^{1/2})} \qquad K_{yy} = \frac{-B'}{[B\rho]_0} + \frac{Q}{2(\Delta y^2 + [\Delta x^2 \Delta y^2]^{1/2})}$$

$$K_{xx1} = -\left[\frac{B'}{[B\rho]_0} + \frac{2Q}{2(\Delta x^2 + [\Delta x^2 \Delta y^2]^{1/2})}\right] \qquad K_{yy1} = -\left[\frac{-B'}{[B\rho]_0} + \frac{2Q}{2(\Delta y^2 + [\Delta x^2 \Delta y^2]^{1/2})}\right]$$

B' = **quadrupole gradient;** $[B\rho]$ = **Ion rigidity** $= p/q$; Q = **perveance** $= \frac{q\lambda}{2\pi\varepsilon_0 \gamma_0^3 m v_{z0}^2}$

We take averages of 2nd, 3rd,... order quantities, forming infinite set of 1st order ode's

$$\frac{d}{ds}\langle x^2\rangle = 2\langle xx'\rangle$$

$$\frac{d}{ds}\langle xx'\rangle = \langle x'^2\rangle + \langle xx''\rangle$$

$$= \langle x'^2\rangle + K_{xx}\langle x^2\rangle + \underline{K_{xx1}\langle x^2\delta\rangle}$$

$$\frac{d}{ds}\langle x'^2\rangle = 2\langle x'x''\rangle$$

$$= 2K_{xx}\langle xx'\rangle + \underline{2K_{xx1}\langle xx'\delta\rangle}$$

$$\frac{d}{ds}\langle x^2\delta\rangle = 2\langle xx'\delta\rangle$$

$$\frac{d}{ds}\langle xx'\delta\rangle = \langle x'^2\delta\rangle + \langle xx''\delta\rangle$$

$$= \langle x'^2\delta\rangle + K_{xx}\langle x^2\delta\rangle + \underline{K_{xx1}\langle x^2\delta^2\rangle}$$

$$\frac{d}{ds}\langle x'^2\delta\rangle = 2\langle x'x''\delta\rangle$$

$$= 2K_{xx}\langle xx'\delta\rangle + \underline{2K_{xx1}\langle xx'\delta^2\rangle}$$

...

$$\frac{d}{ds}\langle x^2\delta^n\rangle = 2\langle xx'\delta^n\rangle$$

$$\frac{d}{ds}\langle xx'\delta^n\rangle = \langle x'^2\delta^n\rangle + \langle xx''\delta^n\rangle$$

$$= \langle x'^2\delta^n\rangle + K_{xx}\langle x^2\delta^n\rangle + \underline{K_{xx1}\langle x^2\delta^{n+1}\rangle}$$

$$\frac{d}{ds}\langle x'^2\delta^n\rangle = 2\langle x'x''\delta^n\rangle$$

$$= 2K_{xx}\langle xx'\delta^n\rangle + \underline{2K_{xx1}\langle xx'\delta^{n+1}\rangle}$$

underline => term higher order by one

PPPL

Infinite set of equations can be truncated, but are reliable over only finite distances

Two equivalent methods of truncation have been employed:

1. $\langle x^2\delta^2\rangle \sim \langle x^2\rangle\langle\delta^2\rangle$ and $\langle xx'\delta^2\rangle \sim \langle xx'\rangle\langle\delta^2\rangle$; or
2. Noticing that $\frac{1}{1+\delta} = 1-\delta+\delta^2+\ldots$ and $\frac{1}{1-\delta} = 1+\delta+\delta^2+\ldots$ thus,

$$\frac{1}{1-\delta}-\frac{1}{1+\delta} = 2\delta+2\delta^3+\ldots \quad \text{also} \quad \frac{\delta}{1+\delta} = 1-\frac{1}{1+\delta}$$

so that we may, to good approximation, write

$$\frac{d}{ds}\langle x^2\rangle = 2\langle xx'\rangle \qquad \frac{d}{ds}\langle xx'\rangle = \langle x'^2\rangle + K_{xx}\langle x^2\rangle + \frac{K_{xx1}}{2}\left[\left\langle\frac{x^2}{1-\delta}\right\rangle - \left\langle\frac{x^2}{1+\delta}\right\rangle\right] + O\left(x^2\delta^3\right)$$

$$\frac{d}{ds}\langle x'^2\rangle = 2K_{xx}\langle xx'\rangle + K_{xx1}\left[\left\langle\frac{xx'}{1-\delta}\right\rangle - \left\langle\frac{xx'}{1+\delta}\right\rangle\right] + O(xx'\delta^3)$$

$$\frac{d}{ds}\left\langle\frac{xx'}{1+\delta}\right\rangle = \left\langle\frac{x'^2}{1+\delta}\right\rangle + K_{xx}\left\langle\frac{x^2}{1+\delta}\right\rangle - K_{xx1}\left\langle\frac{x^2}{1+\delta}\right\rangle + K_{xx1}\langle x^2\rangle \qquad \frac{d}{ds}\left\langle\frac{x^2}{1+\delta}\right\rangle = 2\left\langle\frac{xx'}{1+\delta}\right\rangle$$

$$\frac{d}{ds}\left\langle\frac{x'^2}{1+\delta}\right\rangle = 2K_{xx}\left\langle\frac{xx'}{1+\delta}\right\rangle + 2K_{xx1}\langle xx'\rangle - 2K_{xx1}\left\langle\frac{xx'}{1+\delta}\right\rangle$$

Truncated set of equations forms closed set.

both methods give nearly identical results for $\langle\delta^2\rangle$ in the regime of interest; similar equations for $\langle x^2/(1-\delta)\rangle$, $\langle xx'/(1-\delta)\rangle$, $\langle x'^2/(1-\delta)\rangle$, and the same set for y; 18 equations total.

Comparison of moment equations with Particle-in-Cell (WARP[1]) simulations (1% velocity spread)

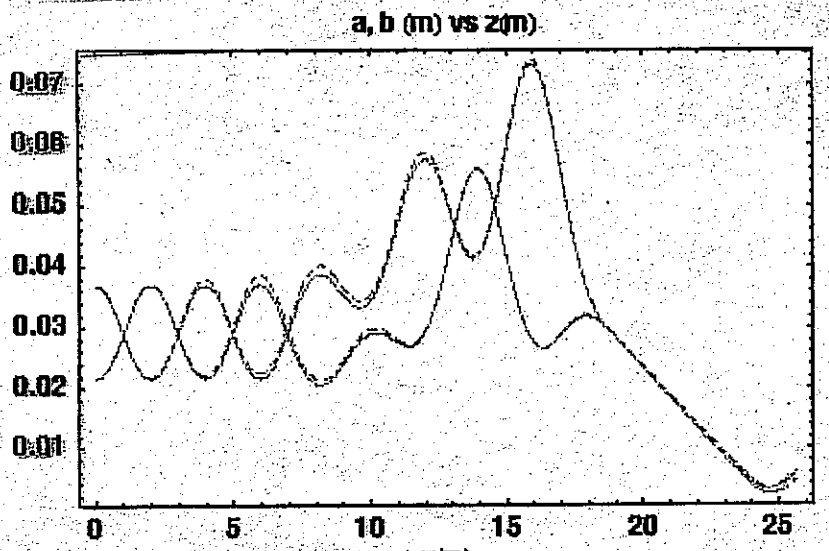

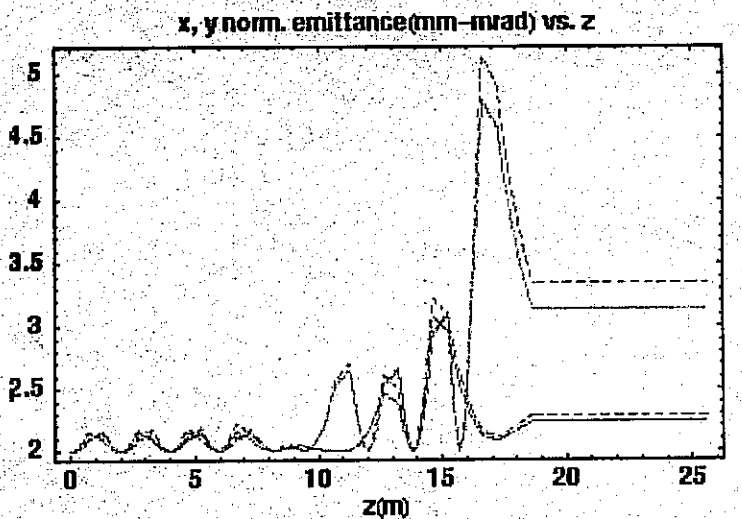

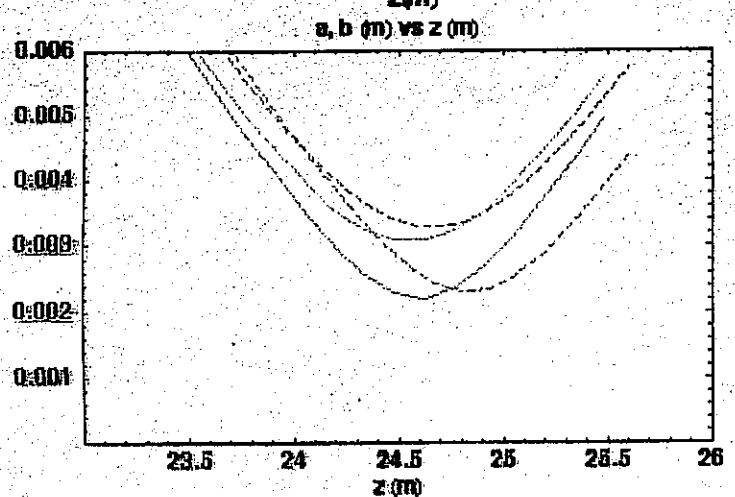

Particle simulations:
Dashed, red (x) and blue (y)
Initial distribution: KV

Moment calculations:
Solid, magenta (x), and aqua (y)

Comparison of moment equations with PIC simulations (WARP) -- no velocity spread

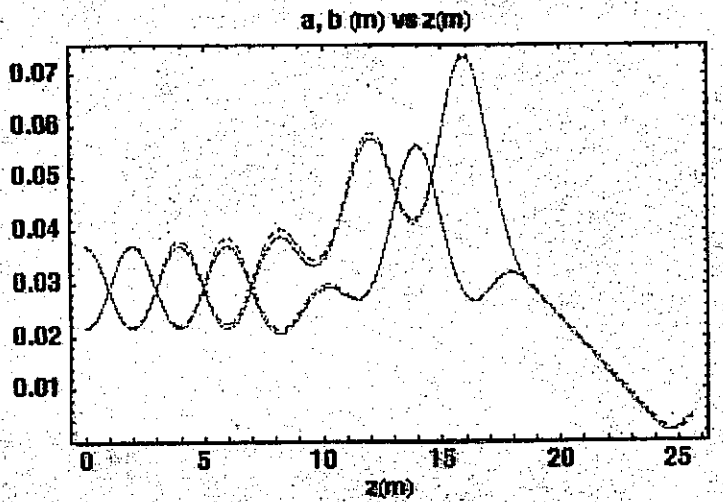

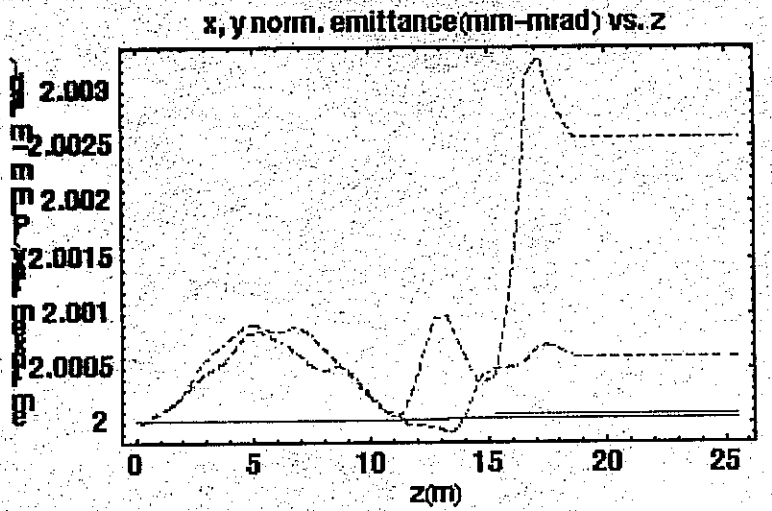

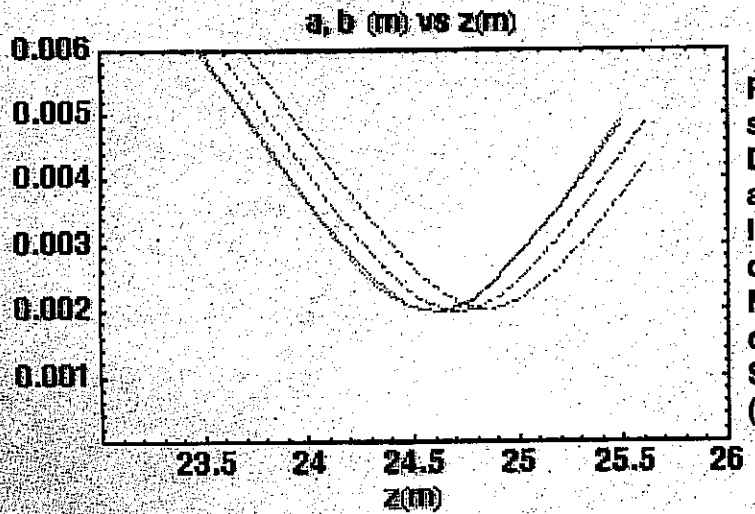

Particle simulations: Dashed, red (x) and blue (y) Initial distribution: KV Moment calculations: Solid, magenta (x), and aqua (y)

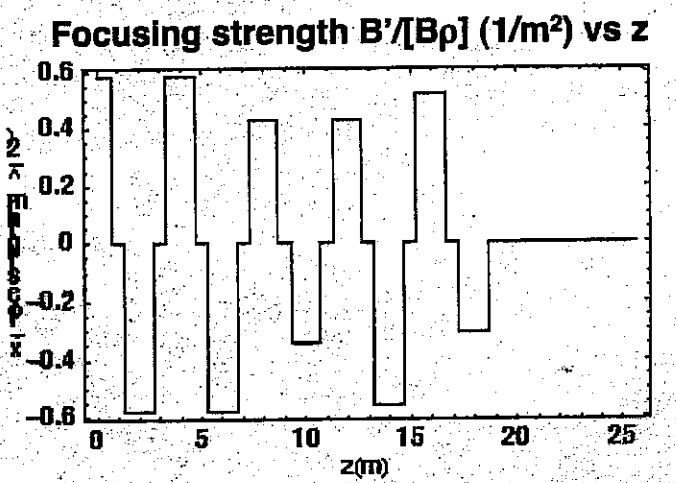

The HIFS VNL has two ongoing experiments, and a long range plan for HEDP studies and Heavy Ion Fusion

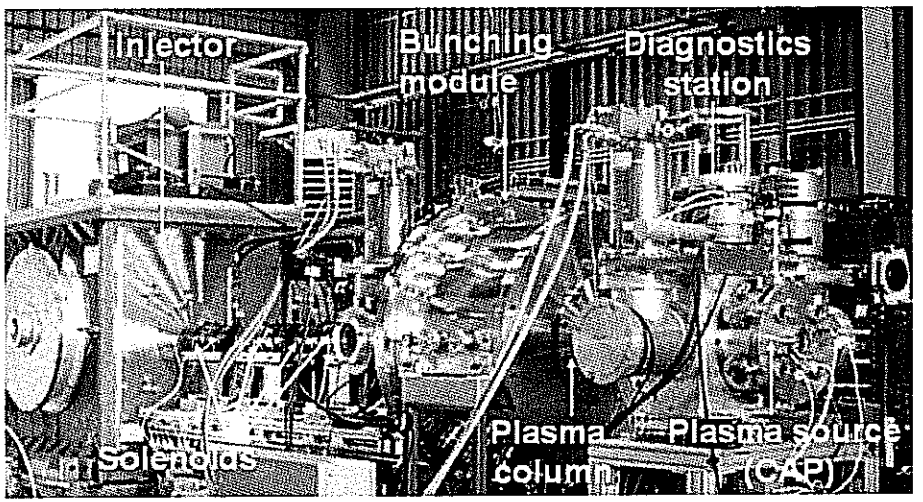

Today:

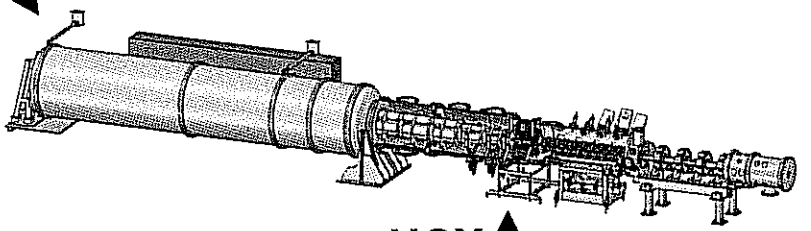

HCX

1.7 MeV, ~0.025 μC

NDCX I

0.4 MeV, 0.003 μC

Soon →

NDCX II 3 - 6 MeV, 0.03 μC

~2009

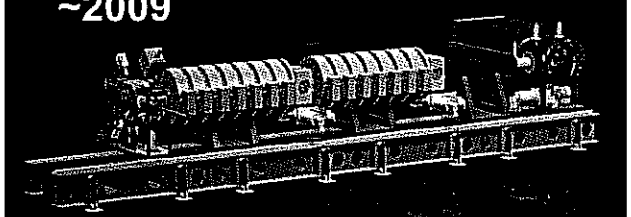

Future

IB-HEDPX (with CD0)

5 - 15 year goal

20 - 40 MeV, 0.3 - 1.0 μC

WDM User facility

10 kJ Machine for HIF

10 - 20 year goal

Target implosion physics

HIF/WDM beam science: neutralized focusing and drift compression are now being tested for use in WDM and HIF

Both techniques virtually eliminate the repulsive effects of space charge on transverse and longitudinal compression

Transverse compression (= focusing the beam to a small spot, raising the watts/cm^2): Recent VNL experiments, eg. scaled final focus experiment, (MacLaren et al 2002), NTX (Roy et al 2004), and current NDCX-1 have demonstrated benefits of neutralization by plasmas, also required for HIF.

Longitudinal compression (= raising the watts): WDM experiments require very short, intense pulses (<~ 1 ns) (shorter than needed for HIF). Neutralization allows high current/high power beams. Modular HIF concept also pushes limit of high current.

NDCX-1 has demonstrated > factor 70 pulse compression, and simultaneous transverse and longitudinal focusing

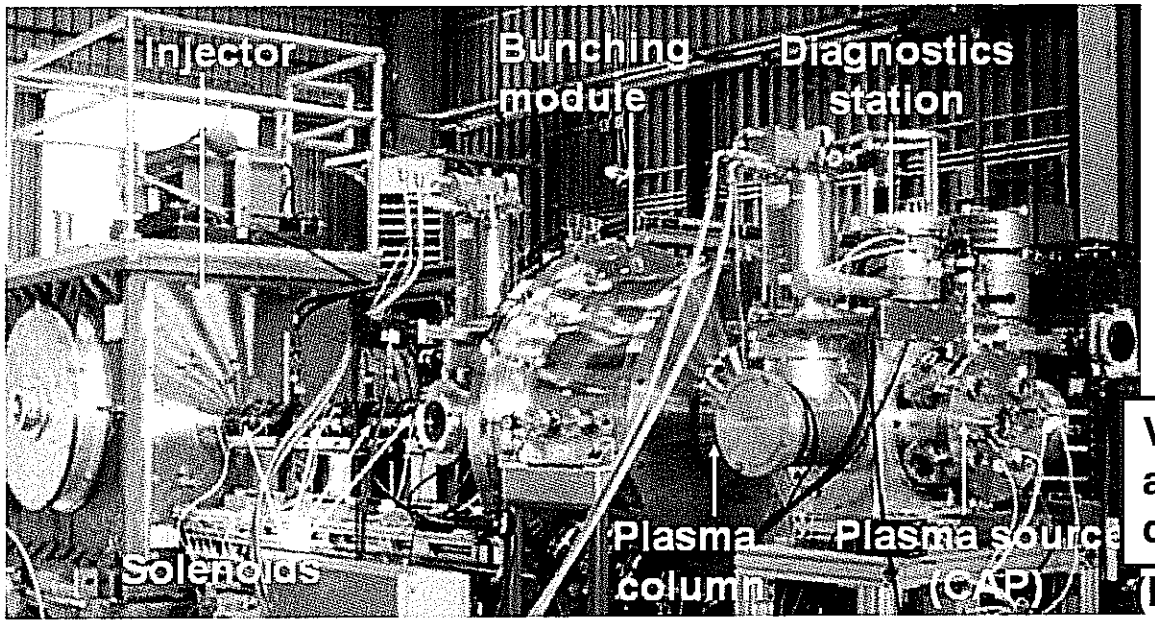

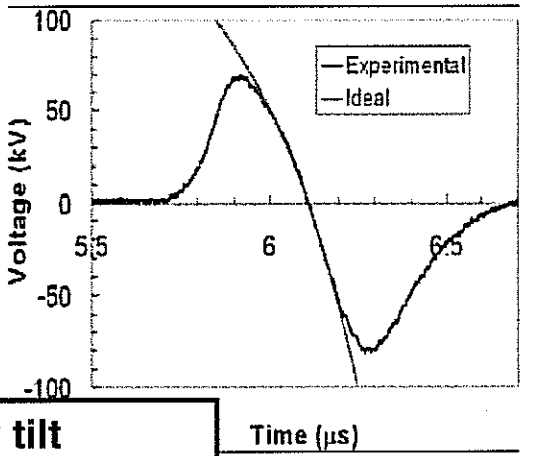

Velocity tilt accelerates tail, decelerates head

(Like chirped pulse compression)

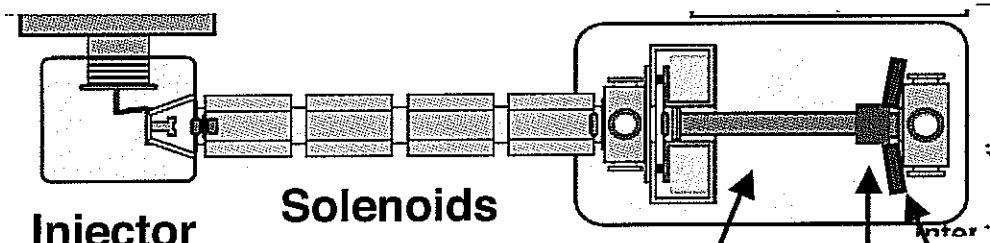

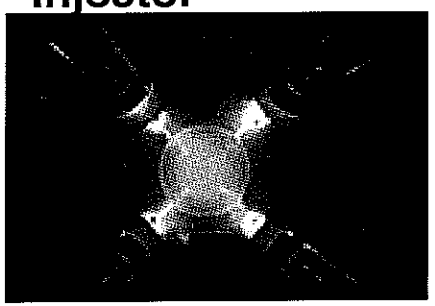

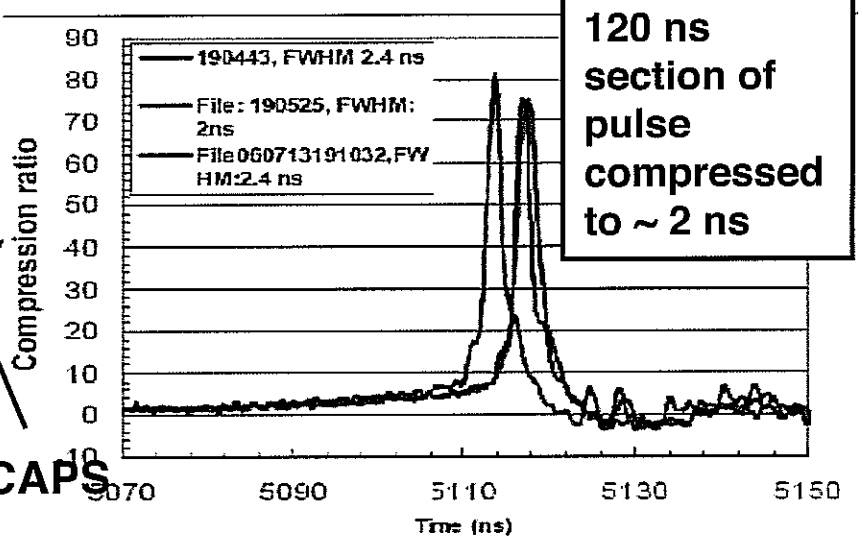

120 ns section of pulse compressed to ~ 2 ns

Artist's Conception of an HIF Power Plant on a few km^2 site

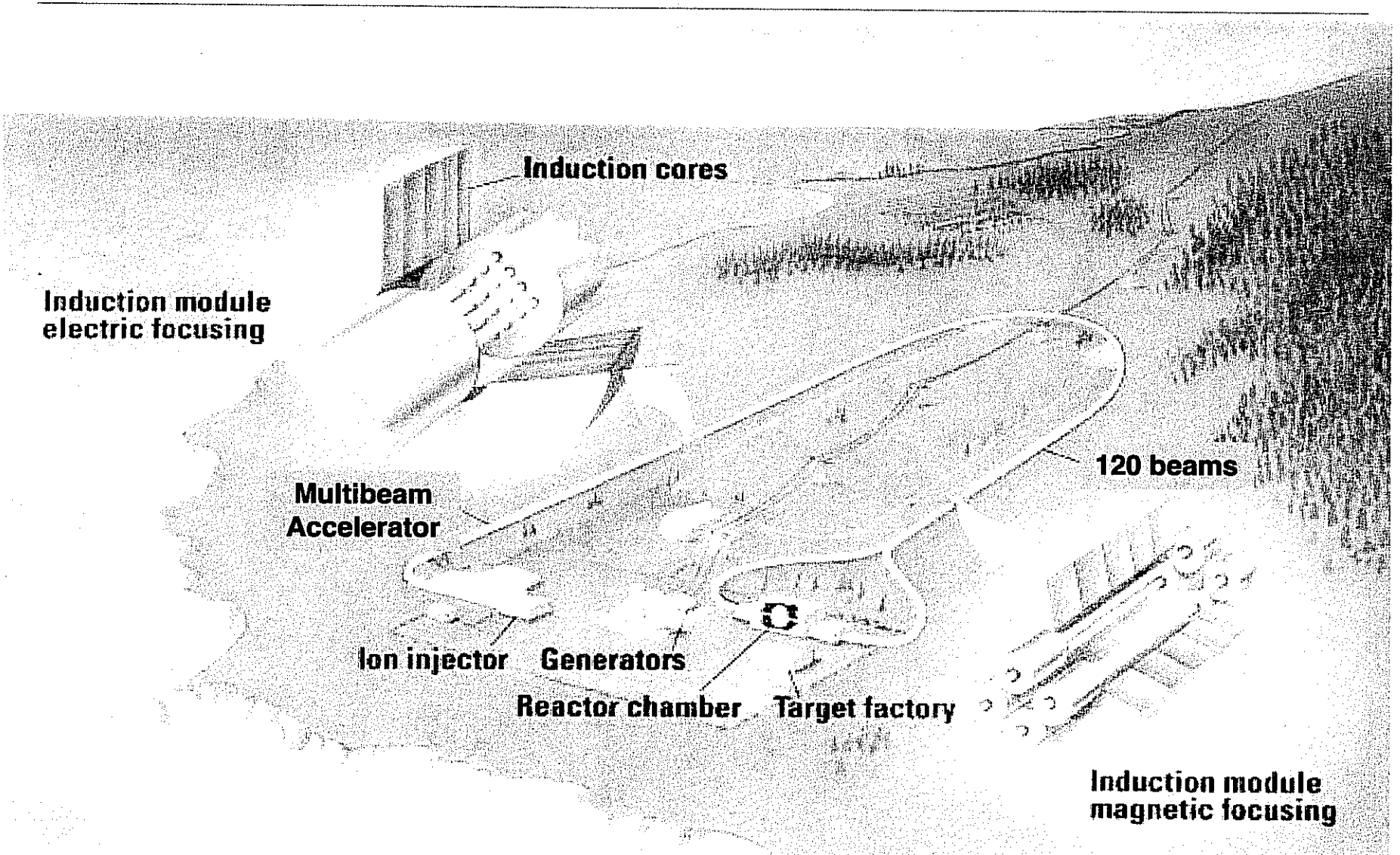

The Heavy Ion Fusion Virtual National Laboratory

PPPL